Celsr2-mediated morphological polarization and functional phenotype of reactive astrocytes in neural repair

Aimei Liu, Lingtai Yu, Xuejun Li, Kejiao Zhang, Wei Zhang, Kwok-Fai So, Fadel Tissir, Yibo Qu, Libing Zhou

Received: 3 December 2022 | Revised: 9 April 2023 | Accepted: 13 April 2023

DOI: 10.1002/glia.24378

GLIA

WILEY

RESEARCH ARTICLE

Celsr2-mediated morphological polarization and functional phenotype of reactive astrocytes in neural repair

Aimei Liu[1,2] | Lingtai Yu[1] | Xuejun Li[1] | Kejiao Zhang[1] | Wei Zhang[1] | Kwok-Fai So[1,2,3,4,5] | Fadel Tissir[6,7] | Yibo Qu[1,4,5] | Libing Zhou[1,2,3,4,5]

[1]Guangdong-Hongkong-Macau CNS Regeneration Institute of Jinan University, Key Laboratory of CNS Regeneration (Jinan University)-Ministry of Education, Guangzhou, People's Republic of China

[2]Neuroscience and Neurorehabilitation Institute, University of Health and Rehabilitation Sciences, Qingdao, Shandong, People's Republic of China

[3]Department of Neurology and Stroke Center, The First Affiliated Hospital & Clinical Neuroscience Institute of Jinan University, Guangzhou, People's Republic of China

[4]Co-innovation Center of Neuroregeneration, Nantong University, Jiangsu, People's Republic of China

[5]Center for Exercise and Brain Science, School of Psychology, Shanghai University of Sport, Shanghai, People's Republic of China

[6]Institute of Neuroscience, Developmental Neurobiology, Université catholique de Louvain, Brussels, Belgium

[7]College of Health and Life Sciences, Hamad Bin Khalifa University (HBKU), Doha, Qatar

Correspondence
Libing Zhou and Yibo Qu Guangdong-Hongkong-Macau Institute of CNS Regeneration, Jinan University, Huangpu Avenue West 601, Guangzhou 510632, People's Republic of China.
Email: tlibingzh@jnu.edu.cn and tquyibo@jnu.edu.cn

Funding information
Guangdong Basic and Applied Basic Research Foundation, Grant/Award Number: 2023B1515040015; Guangdong grant 'Key technologies for treatment of brain disorders', Grant/Award Number: 2018B030332001; Guangzhou Key Projects of Brain Science and Brain-Like Intelligence Technology, Grant/Award Number: 20200730009,20220600003; National Natural Science Foundation of China, Grant/Award Number: 82271400,81971148,82222018; Programme of Introducing Talents of Discipline to Universities, Grant/Award Number: B14036

Abstract

Neural repair is highly influenced by reactive astrocytes. Atypical cadherin Celsr2 regulates neuron development and axon regeneration, while its role in glial cells remains unexplored. In this study, we show that Celsr2 is highly expressed in spinal astrocytes of adult mice, and knockout of *Celsr2* results in reactive astrocytes with longer protrusions preferentially orientated towards lesion borders in culture scratch assay and injured spinal cord, and elevation of total and active Cdc42 and Rac1 protein in western blots. Inactivation of *Celsr2* enhances calcium influx in reactive astrocytes in time-lapse imaging. Morphological phenotypes of cultured *Celsr2*$^{-/-}$ astrocytes are rescued by Cdc42 or Rac1 inhibitors. Following spinal cord injury (SCI), *Celsr2*$^{-/-}$ mice exhibit smaller lesion cavity and glial scar, enhanced fiber regeneration, weaker microglial response, and improved functional recovery than control animals. Similar phenotypes are found in mice with conditional knockout of *Celsr2* in astrocytes. In *Celsr2*$^{-/-}$ mice, astrocyte phenotype is changed and neuroinflammation is alleviated after injury. Inhibiting Cdc42/Rac1 activities compromises astrocyte polarization and the improvement of neural repair and functional recovery in *Celsr2*$^{-/-}$ mice with SCI. In conclusion, Celsr2 regulates morphological polarization and functional phenotype of reactive astrocytes and inactivating *Celsr2* is a potential therapeutic strategy for neural repair.

Abbreviations: BMS, Basso Mouse Scale; BSA, bovine serum albumin; CNS, central nervous system; DIV, Days in vitro; DMEM-F12, Dulbecco's modified Eagle's medium-F12; FBS, fetal bovine serum; GFAP, glial fibrillary acidic protein; HBSS, Hanks' balanced salt solution; KO, knockout; LDs, lipid droplets; LPS, Lipopolysaccharide; MEP, motor-evoked potential; PBS, phosphate-buffered saline; PCP, planar cellular polarity; RT-qPCR, quantitative real-time PCR; SCI, spinal cord injury; MRI, magnetic resonance imaging; FA, fractional anisotropy; DTI, diffusion tensor imaging; RD, radial diffusivity.

Aimei Liu, Lingtai Yu, and Xuejun Li contributed equally to this work.

KEYWORDS
astrocyte phenotypes, astrocyte polarization, atypical cadherins, calcium, neural repair, small GTPase, spinal cord injury

1 | INTRODUCTION

Astrocytes provide neurons with metabolic and structural support and assist the formation of the blood–brain barrier and neural circuits in the central nervous system (CNS) (Santello et al., 2019; Souza et al., 2019). Reactive astrogliosis serves as a neuropathologic hallmark of spinal cord injury (SCI) and plays a dual role in neural repair (Bradbury & Burnside, 2019; O'Shea et al., 2017). Upon injury, reactive astrocytes extend protrusions, migrate at the borders of the lesion, and organize into a barrier-like structure. In acute and subacute phases of SCI, reactive astrocytes efficiently isolate the damaged tissue and secrete molecules such as laminin, fibronectin, tenascin C, and proteoglycans that affect neuronal outgrowth (Anderson et al., 2016; Bush et al., 1999; Yang et al., 2020). Simultaneously, astrocyte protrusions are radially extended and repetitively twined to form glial scar as the physical barrier for axon regrowth (Bradbury & Burnside, 2019; Silver & Miller, 2004). Modulation of astrocyte behavior after injury offers potential prospect for neural repair. Inhibition of the STAT-3 signaling impairs the formation of the scar border by proliferative, elongated astrocytes and hampers the healing of SCI lesions (Okada et al., 2006; Wanner et al., 2013). The orderly arrangement of reactive glial protrusions potentially limits scar formation and might be important for lesion healing and axon regeneration.

Morphological polarization is an important characteristic of migrating reactive astrocytes, with reorganization of microtubule organization centers, cytoskeleton and Golgi complex facing the lesion (Etienne-Manneville & Hall, 2001). Small GTPases Cdc42 and Rac1 are key regulators of cell polarization by modulating actin cytoskeleton dynamics and reorganization (Fukata et al., 2003). They regulate protrusion formation and cell orientation by recruiting the Par6/aPKC polarity complex, with Cdc42 initiating the formation of protrusions and Rac1 regulating their elongation (Etienne-Manneville & Hall, 2001). The localization and activity of Cdc42 during astrocyte polarization are regulated by Scrib which influences APC and Dlg1 recruitment to the leading edge to promote polarization (Osmani et al., 2006). After SCI, inhibition of the β1-integrin and Wnt/β-catenin pathways shortens the length of protrusions of polarized astrocytes, and decreases the percentage of astrocytes oriented perpendicular to the lesion (Sonn et al., 2020). N-cadherin levels affect wound-induced integrin-mediated recruitment of Cdc42 to modulate astrocyte polarization and migration (Camand et al., 2012).

Besides morphological polarization, reactive astrocytes have been functionally classified into A1 and A2 phenotypes (Liddelow et al., 2017). Activated microglia-secreted cytokines may induce A1 reactive astrocytes which are abundant in the brain of patients with many neurodegenerative disorders and characterized by the expression of complement component C3, while A2 astrocytes are C3 negative and strongly promote neuronal survival and tissue repair. After SCI, modulating the A1-to-A2 phenotype switch of reactive astrocytes significantly contributes to neural repair and functional recovery (Su et al., 2019; Vismara et al., 2020).

Celsr1, 2, and 3 are three mammalian orthologs of *Drosophila Flamingo* that form a family of atypical cadherin anchored to membranes by seven helical segments. *Flamingo* is a planar cell polarity (PCP) gene that works together with other members including *Frizzled* and *Vangl* to coordinate morphogenetic behaviors of individual cells and cell populations with embryonic polarity (Gray et al., 2011). In mammals, the roles of *Celsr2* and *Celsr3* are complementary and partly redundant (Qu et al., 2010; Qu et al., 2014; Tissir et al., 2010). Genetic evidence indicates that *Celsr3* plays a prominent role in axon pathfinding, whereas *Celsr2* is more critical for ependymal cilia polarity and neuronal migration (Feng et al., 2012; Goffinet & Tissir, 2017). Our recent study shows that *Celsr2* inactivation in spinal motoneurons promotes axon regeneration in a cell autonomous manner by upregulating Cdc42/Rac1 signaling in mouse and human (Wen et al., 2022), indicating that Celsr2 acts a potential player in neural repair (Petrova & Hakim, 2022). Single-cell RNAseq data show that astrocytes also express Celsr2 (Zhang et al., 2016), raising the possibility that Celsr2 in astrocytes might influence neural repair.

To test this hypothesis, Celsr2 expression was studied in intact and injured adult spinal cords using *Celsr2*^{LacZ} mice. The effect of *Celsr2* inactivation on reactive astrocytes was analyzed in culture using wound scratch and chemotaxis assay, and in lesion borders after SCI. The involvement of Cdc42/Rac1 signaling in Celsr2-mediated mobility of reactive astrocytes was assessed in cultured cells and injured spinal cords. Using SCI models, we compared lesion healing, axon regeneration and functional recovery, and microglial response and cytokine production in lesion areas, in control and *Celsr2*$^{-/-}$ mutant mice. A cell-autonomous role of Celsr2 in regulating reactive astrocytes to influence neural repair and functional improvement was verified using SCI in mice with astrocyte-specific *Celsr2* inactivation. Functional phenotypes were tested by the expression markers in reactive astrocytes, and neuroinflammation was assessed in injured spinal cords. Our studies indicate that loss of atypical cadherin *Celsr2* contributes to astrocyte morphological polarization and A2 functional phenotype, which are beneficial for neural repair and functional recovery after SCI.

2 | MATERIALS AND METHODS

2.1 | Animals

Animal experiments were approved by the Laboratory Animal Ethics Committee at Jinan University. *Aldh1l1-CreER*^{T2} mice were provided by Hu et al. (2020), and the generation of *Celsr2*$^{-/-}$, *Celsr2*$^{f/f}$, and *Celsr2*^{LacZ} mice was described previously (Tissir et al., 2010). Animals of *Aldh1l1-CreER*^{T2} and *Celsr2*$^{-/-}$ were crossed to generate

Aldh1l1-CreER^{T2}; *Celsr2*$^{+/-}$ males, and they were further crossed with *Celsr2*$^{f/f}$ females to produce *Aldh1l1-CreER*^{T2}; *Celsr2*$^{f/-}$ mice, to increase the recombination efficiency (Zhou et al., 2008). These mice were subjected to intraperitoneal injection of tamoxifen (100 mg/kg) once a day (Hu et al., 2020) to conditionally inactivate one *Celsr2* allele in astrocytes and short as *Celsr2* c KO. All mice were from C57/B6 background. Animals were housed at 23 ± 1°C, 12-h dark/light cycle.

2.2 | Primary spinal astrocyte culture

Astrocyte cultures were prepared from neonatal mice at postnatal day 1–3. In Hanks' balanced salt solution (HBSS, Thermo Fisher Scientific, MA, USA), spinal cord tissues were dissected out and meninges were peeled away. After trypsinization (0.15% trypsin, 7 min, 37°C) and centrifugation (200 g, 5 min), dissociated spinal cells were suspended in astrocyte culture medium consisting of Dulbecco's modified Eagle's medium-F12 (DMEM-F12; Gibco, New York, USA) and 10% fetal bovine serum (FBS, Gibco), plated in T75 flasks and then cultured in a 37°C, 5% CO_2 incubator. When cells reached confluence (about 9–12 days in vitro), the flasks were shaken at 200 rpm for 20 h to detach neurons, microglia, and oligodendrocytes. The cells were washed with the astrocyte culture medium, trypsinized and reseeded. Astrocyte purity was evaluated by rat anti-glial fibrillary acidic protein (GFAP; 1:1000, 13-0300, Themor Fisher Scientific) immunostaining and DAPI nucleus stain, and astrocytes with a purity higher than 95% were used in the subsequent studies.

2.3 | Wound scratch assay

Purified astrocytes were seeded on poly-D-lysine-coated coverslips (50 μg/mL) at a density of 1.2×10^4 cells/coverslip, in 12-well plates. Once confluency reached more than 80%, astrocytes were serum-starved overnight, and monolayers were scratched with a 200 μL-pipette tip. After washing to remove debris, astrocytes were cultured for different time. To study cell protrusion length and angle of extension relative to the scratching line, cultures were stopped at 16 h, and cells were fixed in 4% paraformaldehyde and followed with anti-GFAP immunostaining. The images were captured with a confocal microscope (LSM700, Zeiss, Germany). To assess astrocyte migration, pictures were taken with a microscope equipped with a 5x objective, bright field, every 24 h for 5 days after scratching. Images were analyzed using Image J. To inhibit Cdc42 or Rac1 activity, cultured astrocytes were incubated with 5 μM ML141 (HY-12755, MCE, New Jersey, USA) or 50 μM NSC23766 (HY-15723A, MCE, NJ, USA) for 24 h before starving and scratching as described (Chaker et al., 2018; Jiang et al., 2020).

2.4 | Calcium imaging

Purified astrocytes were seeded on coverslips at the density of 3×10^4 cells/coverslip. After 3 days in vitro (DIV), cultures were incubated in HBSS with 5 μM Fura-4 AM (DOJINDO Chemical Technology) for 30 min at room temperature. Coverslips were transferred to a glass-bottom chamber under an inverted microscope (Axioplan2, Zeiss, Germany) and perfused with the calcium-imaging buffer. Cultured astrocytes were stimulated by 100 μM ATP for 5 minutes and images of individual cells were captured from 3 min before to 13 minutes after the stimulation (one picture every 3 sec) for analysis of the fluorescence intensity peak. A total of 32 control and 27 mutant cells were analyzed.

2.5 | Chemotaxis assay

Using transwell chambers with 8-μm-pore membrane (Corning, New York, USA) in 24-well plates, macrophages (RAW 264.7, 3.5×10^5 cells/ml) were seeded into the lower chambers in 10% FBS-DMEM/F12 medium (Gibco), and 4 h later treated with lipopolysaccharide (LPS, 200 ng/mL, Themor Fisher Scientific) for 24 h. Thereafter, astrocytes (9×10^4 cells/ml) were seeded in the upper chambers and maintained for 20 h at 37°C with 5% CO_2. The membranes were fixed with 4% paraformaldehyde for 10 min and then stained with Hoechst 33258 (Themor Fisher Scientific). Cells on the upper side of the membrane were removed using a cotton swab and astrocytes on the lower face were imaged using a confocal microscope equipped with 10x objective.

2.6 | EdU labeling

Purified astrocytes (1.2×10^5 cells/ml) were seeded on 18-mm coverslips coated with poly-D-lysine (50 μg/mL). After 24 h of incubation with medium conditioned by macrophages (RAW 264.7) stimulated by LPS (200 ng/mL), astrocytes were treated by 10 μM EdU (EdU Cell Proliferation Kit with Alexa Fluor 555, BeyoClickTM) for 24 h. They were then fixed with 4% paraformaldehyde for 15 minutes, washed with phosphate-buffered saline (PBS) containing 3% bovine serum albumin (BSA), and incubated with the Click Additive buffer for 15 min. Hoechst 33342 was used to stained nuclei.

2.7 | Contusion SCI models

After anesthetization with 4% sodium pentobarbital (50 mg/kg; Beyotime Biotechnology, China), a laminectomy at T8 was performed to expose the spine of T10 with the dura mater intact. After immobilization with a spine stabilizer, T10 spinal segment was injured using a LISA impactor with a height of 0.4 mm and a contact duration of 0.4 sec. To study the effect of the Cdc42/Rac1 signaling involved in *Celsr2* inactivation, *Celsr2*$^{-/-}$ mice with SCI were subjected to intraperitoneal injection of Rac1 inhibitor (NSC23766; 10 mg/kg/day; MCE) and Cdc42 inhibitor (ML141; 3.5 mg/kg/day; MCE) once a day for 14 consecutive days as previously described (Li et al., 2019; Liao et al., 2014). The same amount of isotonic saline was applied in

controls. Mice with a Basso Mouse Scale (BMS) score of more than 0 on the second day post-surgery were excluded, and the others received intramuscular gentamicin (5 mg/kg) for 3 days. Bladders were emptied twice a day until mice could urinate freely. All animals were housed in a controlled room (22°C–24°C, light/dark cycle for 12 h).

2.8 | Mouse hemisection models

Young adult mice (6 weeks old) were anesthetized with 4% sodium pentobarbital (50 mg/kg; Beyotime Biotechnology, China). The spinous process and the vertebral lamina were removed to expose the spinal cord at T10 level. The central blood vessel was compressed to prevent bleeding, and right halves of spinal cords were transected using a Nordland blade (N-6900, American MasterTech). After surgery, gentamicin (5 mg/kg; Guangdong Bangmin Pharmaceutical, Jiangmen, China) was administered for 3 days.

2.9 | Behavioral tests

BMS scores: Basic locomotor function was evaluated by two observers using BMS scores that range from 0 (complete paralysis) to 9 (completely normal) during first 3 days and then weekly after surgery. Mice were placed in an open field and observed individually for 5 min. The final BMS score was the average of the two independent raters.

Heat hyperalgesia: Heat hyperalgesia was assessed by a radiant thermal stimulus (Series8/Model 390, IITC Life Science). Before testing, mice were conditioned in the test box for at least 2 h. The plantar surfaces of hindpaws were stimulated with a temperature from 30°C to 50°C. Each mouse was stimulated 6 times with intervals of 5 minutes, and the withdrawal latency was the average time.

Grid tests: Mice were placed on a wire mesh to count the footslips of the hindlimbs in 50-step walking. A partial footfault (score of 1) was when hindlimbs slipped without touching the glass and full footfault (score of 2) when hindlimbs slipped and touched the glass. The foot-fault rate was calculated as (partial footfault * 1+ full footfault * 2)/50 (total number of steps) * 100% (Britt et al., 2010).

Catwalk tests: Animals were adapted in the dark and a quiet environment for 2 h before testing. Each mouse walked along a 50-cm-long glass panel for at least 3 times and the footprints were recorded by the camera under the glass. The walking parameters were analyzed automatically. Walking coordination were estimated by the Regularity Index and the maximal area of contact between the paw and the glass (Koopmans et al., 2005).

2.10 | Motor-evoked potential (MEP) recordings

Mice were immobilized in a stereotactic apparatus under propofol anesthesia (20 μL/g). The stimulation electrode was inserted into the motor cortex, and the recording electrode was applied to the gastrocnemius muscle. Upon a pulse (3500 mV stimulus of 0.2 ms at 1 Hz) stimulation, the MEP was recorded by a Keypoint Portable device (Dantec Biomed, Denmark) with a 30 Hz to 3 kHz bandpass filter.

2.11 | Rac1/Cdc42 activity assay

Proteins were extracted from mouse spinal samples (T9-T11 segments) 7 days after contusion and from cultured spinal astrocytes 24 h treated with the macrophage-conditioned medium, GTP-bound Cdc42 and Rac1 were estimated using a Rac1/Cdc42 Activation Assay Kit (#17–441, Merck Millipore). Briefly, samples were homogenized in the lysis buffer (125 mM HEPES (pH 7.5), 750 mM NaCl, 5% Igepal CA-630, 50 mM MgCl2, 5 mM EDTA, 10% glycerol and protease inhibitors). Lysates were incubated with glutathione-agarose beads conjugated with the Rac1 or Cdc42 Protein Binding Domain fused to GST, at 4°C for 60 min and the beads were washed three times in lysis buffer. GTP-bound proteins were eluted in sample gel buffer and subjected to western blots.

2.12 | Western blots

Protein extracts from spinal samples, cultured spinal astrocytes, and the proteins eluted from glutathione agarose beads were analyzed on 10% sodium dodecylsulfate polyacrylamide gels and transferred to 0.45 μm polyvinylidene fluoride membranes. The following primary antibodies were used: anti-β-III tubulin rabbit polyclonal antibody (1:1000; ab18207, Abcam), anti-GAPDH mouse polyclonal antibody (1:1000; ab8245, Abcam), anti-Rac1 mouse polyclonal antibody (1:1000; 610650, BD Pharmingen), anti-Cdc42 rabbit polyclonal antibody (1:1000; 11A11, CST); the secondary antibodies were peroxidase anti-rabbit IgG (1:5000, ab6721, Abcam) and peroxidase anti-mouse IgG (1:10,000; Vector Laboratories). Immunoreactivity was detected using an enhanced chemiluminescence detection kit (1705061, Bio-Rad); images were captured using the ChemiDoc™ Touch Imaging System (Bio-Rad), and signals were quantified using ImageJ. The ratios of total Cdc42 or Rac1 to reference proteins in each sample and the average ratios in control samples were calculated, and all data were then normalized to the control average ratio correspondingly.

2.13 | Cytokine analysis

Three and 7 days after SCI, spinal segments (1 cm long) surrounding injury sites were collected for cytokine analysis. Samples were homogenized in RIPA (P8340-1, Solarbio Bioscience and Technology, Beijing, China) and cytokine levels were measured by the Bio-plex system (BioRad) using a 23-plex cytokine kit (catalog no. M60009RDPD, BioRad, CA, USA), which included antibodies against TNF-α, MCP-1, MIP-1α, MIP-1β, RANTES, IFN-γ, G-CSF, GM-CSF, IL-1α, IL-1β, IL-2,

IL-3, IL-4, IL-5, IL-6, IL-9, IL-10, IL-12 (p40), IL-12 (p70), IL-13, IL-17A, Eotaxin and KC. Three animals were used in each group at each timepoint.

2.14 | Immunofluorescent staining

After perfusion with 4% paraformaldehyde, spinal segments (about 1 cm around injury regions) were collected for preparing serial transverse (20–40 μm thickness) or horizontal cryostat sections (15-μm thickness). Primary antibodies were rat anti-GFAP (1:1000; 13–0300, Themor Fisher), rabbit anti-Olig2 (1:1000; ab9610, Millipore), mouse anti-NeuN (1:1000; ab104224, Abcam), rat anti-CD68 (1:1000; ab53444, Abcam), rabbit anti-serotonin (5-HT; 1:1000, s5545, Sigma), chicken anti-β-gal (1:1000; ab9361, Abcam), rabbit anti-Iba1(1:1000; 019–19741, Wako), rat anti-C3 (1:1000; ab11862, Abcam). Fluorescent Alexa Fluor 488, 546 and 647 secondary antibodies (1: 1000; A21202/A10040/A31571, Themor Fisher) were used to disclose signal. For double labelling of lipid droplets in contusion SCI models, sections were washed once and incubated with BODIPY 493/503 (1:1000; D3922, Thermo Fisher) for 15 min at room temperature.

2.15 | Image analysis

Images were captured with a fluorescence microscope (Imager Z2, Zeiss) or a confocal microscope (LSM700, Zeiss) and analyzed using ImageJ. In each spinal block, 5 series of sections were prepared with a spacing between adjacent sections of 100 μm (transverse sections) or 75 μm (horizontal sections). The alternate sections in each series were subjected to double and triple immunostaining. All stained sections were used for analysis.

Cell densities: In hemisection model, the numbers of Iba1-cells were calculated in lesion areas (0.5 mm × 0.5 mm). In contusion models, Iba1-positive and EdU-positive cells were counted in three frames (0.5 mm × 0.5 mm) chosen randomly in dorsal spinal cord areas using ImageJ, at +3 mm from the injury epicenter; the numbers of lipid droplet (LDs), BODIPY-positive /Iba1-positive cells and C3-positive astrocytes were manually counted in three frames (0.5 mm × 0.5 mm) at the lesion level. Four or five animals were used in each group.

Fiber density: Horizontal lines perpendicular to the longitudinal axis of spinal cord were drawn at different distances from the injury center. The number of 5-HT-positive fibers intercepting lines was counted (length > 10 μm) as described (Anderson et al., 2018). The average intercepts per section at different distances from the injury center in each animal were estimated, and five animals were used in each group.

Polarization analysis: In spinal sections after SCI, the length of astrocytic protrusions in areas 250 μm away from lesion cores was measured, between nuclei as the starting point and the furthest protrusion tip. Astrocytes were considered polarized if their morphology was asymmetrical with obvious long protrusions. The transverse axis of the lesion was used as the reference direction, and the largest value of 90° indicated that astrocyte protrusion was directed towards the lesion core (Sonn et al., 2020).

Glial scar: Glial scar were quantified using the ImageJ in serial transverse spinal cord sections stained for GFAP at different distances from the injury center.

2.16 | Reconstruction of lesion cavity

In individual horizontal spinal sections, lesion area was visualized according to GFAP immunostaining. In each spinal sample, five serial sections spaced 90 μm were reconstructed to calculate lesion volume using Neurolucida (MBF Bioscience, Williston, VT, USA). Five animals were used in each group.

2.17 | Quantitative real-time PCR (RT-qPCR)

Total RNA of spinal samples or cultured astrocytes stimulated by the macrophage-conditioned medium for 24 h was extracted using the TriZol Reagent (Invitrogen, Carlsbad, CA, USA) according to the manufacturer. cDNA was synthesized from total 1 μg RNA using the Reverse Transcription System (Promega) and 1 μL cDNA subjected to PCR using the Eco™ Real-Time PCR System (illumina). Primers were list in Table S1. The expression level was evaluated using the 2-ΔΔCt method.

2.18 | Experimental design and statistical analysis

Results are presented as mean ± SEM. Two-way repeated measures ANOVA with Bonferroni's *post hoc* correction was used for comparisons of BMS scores at different timepoints and volumes at different distances to lesion epicenters. Chi-square test was used for the statistical analysis of protrusion's orientation. Other data were analyzed using Student's *t*-test or one-way ANOVA analysis of variance with Tukey's multiple comparison tests (Prism®, 7.0c, GraphPad, San Diego, CA, USA). The significance level was set as $P < 0.05$.

3 | RESULTS

3.1 | *Celsr2* inactivation enhances astrocyte polarization and migration in vitro

To assess a putative role of Celsr2 in glial cells, we first studied Celsr2 expression in adult spinal cords using anti-β-gal immunostaining in *Celsr2*^{LacZ} transgenic mice (Tissir et al., 2010). Double immunofluorescent staining showed that β-gal signal was present in all GFAP-positive astrocytes (Figure 1a) and some Olig2-positive oligodendrocytes (Figure S1A), but not in Iba1-positive microglial cells (Figure S1B). To study Celsr2 expression in injured spinal cord, we

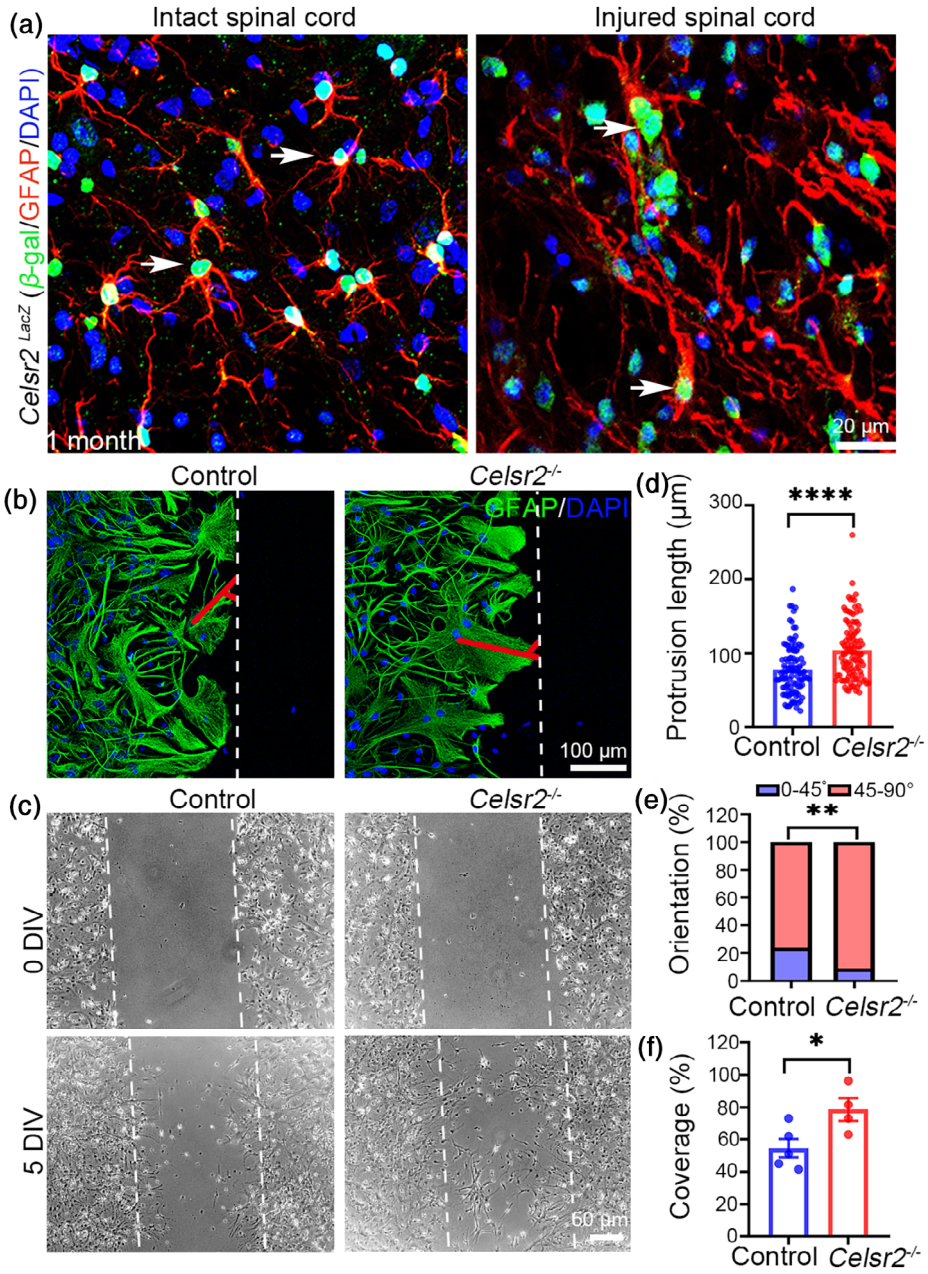

FIGURE 1 *Celsr2* negatively regulates astrocyte polarization and migration in vitro. a. Immunostaining of transverse sections of intact and injured spinal cords from 1-month-old *Celsr2*^{LacZ} transgenic mice. β-gal signal (green) is present in all GFAP-positive (red) quiescent and reactive polarized astrocytes (arrows). b–f. Astrocyte reactivity is studied in cultured cells followed with wound scratch assay. At 16 h after scratch, GFAP immunostaining shows protrusions of polarized astrocytes (b), and a significant increase of protrusion length in the *Celsr2*$^{-/-}$ compared to the control (d; $n = 102$ and 106 cells in the control and the mutant). Protrusion orientation is evaluated by the angles between protrusion axes and the scratch line (indicated in b) and shows that more astrocytes with protrusions preferentially oriented perpendicular to the lesion (45°–90°) in mutants compared to controls (e; 109/120 vs. 91/119). After 5 DIV, the coverage of migrating astrocytes in lesion areas is significantly increased in the mutant (c, f; $n = 5$ and 4 objective fields in the control and the mutant, respectively). d, e. Three independent experiments; f. Four independent experiments; one dot in f represents the average of one experiment. $^{*}P < 0.05$; $^{**}P < 0.01$; and $^{****}P < 0.0001$; Student's *t*-test in d and f; Chi-square test in e.

performed a contusion at T10 spinal segment in adult *Celsr2*^{LacZ} mice and analyzed lesioned spinal samples 7 days after injury. Around the lesion, reactive astrocytes with long protrusions were positive for β-gal (Figure 1a). Notably, a few activated, rounded Iba1-positive microglia also expressed β-gal (Figure S1C), which was confirmed by staining for the macrophage/microglia marker CD68 (Figure S1D). Since Celsr2 is highly expressed in both quiescent and reactive astrocytes, we focused our study on these cells.

We then examined the effect of *Celsr2* inactivation on astrocyte response in vitro. In a monolayer of astrocytes, scratch induced the formation of astrocyte protrusions in control and *Celsr2*$^{-/-}$ samples (Figure 1b), but the protrusions were longer in *Celsr2*$^{-/-}$ mutants than in controls (Figure 1d; control and mutant: 78.2 ± 3.5 and 104.1 ± 3.9 μm, 102 and 106 cells, $P < 0.0001$; Table S2). The percentage of astrocytes with protrusions preferentially oriented perpendicular to the lesion (45°–90°) was significantly increased in the mutant compared to the control (Figure 1e; control and mutant: 91/119 and 109/120, $P < 0.01$).

To assess whether Celsr2 is involved in astrocyte migration, we carried out wound scratch assay (Figure 1c). After 5 DIV, the coverage of migrating astrocytes in lesion areas was significantly increased in *Celsr2*$^{-/-}$ mutant monolayers (Figure 1f; control and mutant: 54.6 ± 5.8% and 78.6 ± 7.0%, five and four replicates, $P < 0.05$; Table S3). In a transwell assay, cultured macrophages were stimulated by LPS to produce chemokines in the lower chamber and astrocytes were seeded in the upper chamber. Hoechst staining showed that a higher number of astrocytes migrated through the membrane pores in *Celsr2*$^{-/-}$ mutant than the control (Figure S2A,B; control and mutant

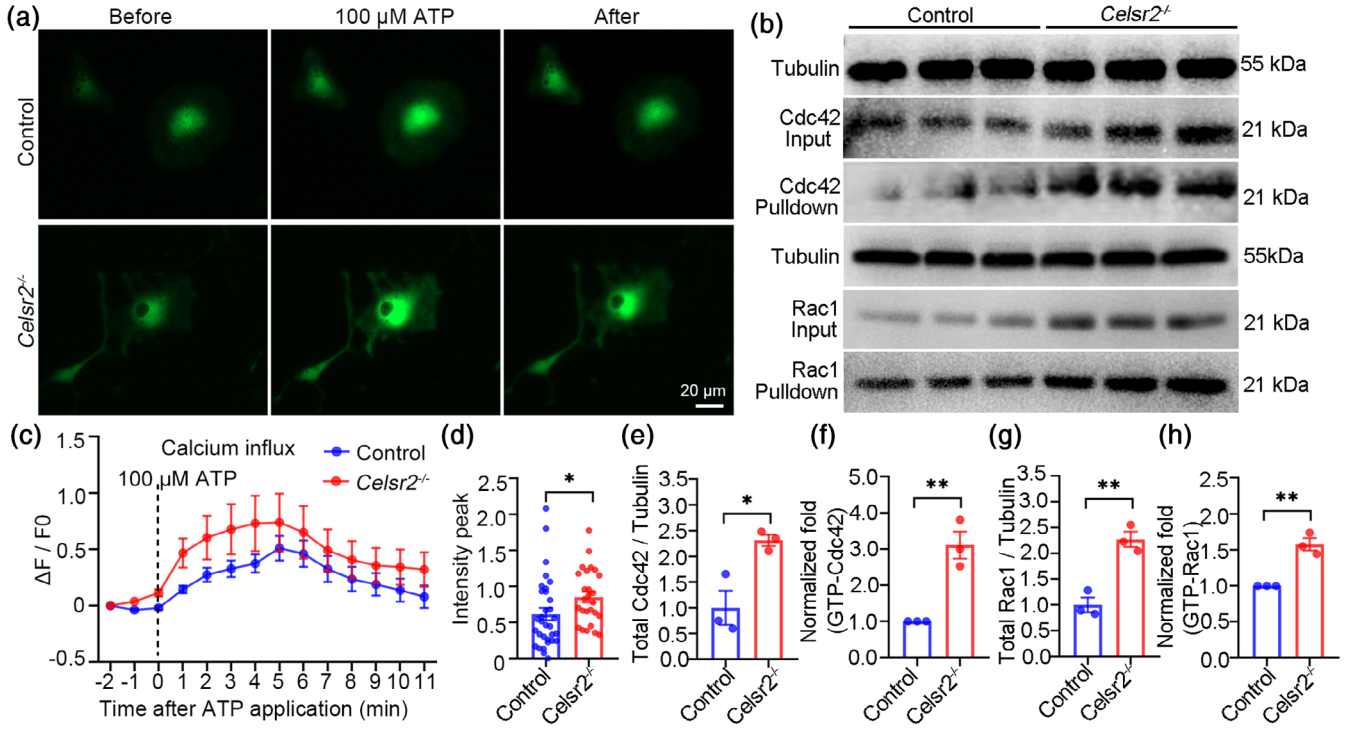

FIGURE 2 *Celsr2* inactivation contributes to intracellular calcium release and enhances Cdc42/Rac1 signaling in cultured spinal astrocytes. a, c, and d. In 3-DIV cultured astrocytes, intracellular calcium followed by Fura-4AM is monitored in individual cells, before and after ATP stimulation (a). Analysis of fluorescence intensity (c) shows a significant increase of intracellular calcium peak in mutants compared to controls (d; $n = 32$ and 27 cells in the control and the mutant). Three independent experiments in each group. b, e–h. Western blot analysis of total protein extracts from cultured astrocytes stimulated by macrophage-conditioned medium for 24 h, or of eluted proteins from GST-bound beads (b). There is a significant increase of total Cdc42 proteins (e), GTP-bound Cdc42 (f), total Rac1 proteins (g) and GTP-bound Rac1 (h) in the mutant compared to the control. Three replicates in each group. *$P < 0.05$; **$P < 0.01$; Student's *t*-test.

in 0.4 mm^2: 6.8 ± 0.7 and 11.6 ± 0.7 cells, $n = 20$ objective fields, $P < 0.0001$). However, EdU labeling showed that astrocyte proliferation stimulated by the macrophage-conditioned medium was comparable in both groups (Figure S2C, D; control and mutant in 0.4 mm^2: 9.2 ± 0.6 and 9.3 ± 0.5 cells, $n = 20$ objective fields, $P > 0.05$). These results suggest that Celsr2 inhibits the polarization and migration of reactive astrocytes.

3.2 | *Celsr2* inactivation increases ATP-stimulated calcium release and Cdc42/Rac1 signaling in cultured spinal astrocytes

Intracellular increase of calcium is necessary for astrocyte polarization and migration (Lagos-Cabre et al., 2018). We compared intracellular calcium release in cultured astrocytes stimulated by the application of 100 μM ATP and found that the peak of calcium activity was significantly increased in *Celsr2*$^{-/-}$ mutant compared to control cells (Figure 2a, c, d; control and mutant: 0.62 ± 0.09 and 0.90 ± 0.09, 32 and 27 cells, $P < 0.05$; Movies S1 and S2).

Small GTPase Cdc42 and Rac1 are key regulators of astrocyte polarization, as inhibition of Cdc42 and Rac1 function in cultured astrocytes impaired protrusion initiation and elongation in a tubulin-dependent manner (Etienne-Manneville & Hall, 2001). To test whether *Celsr2* knockout impacts Cdc42/Rac1 signaling, cultured astrocytes were stimulated by macrophage-conditioned medium, and proteins were analyzed by western blot. As predicted, there was a significant increase of total and GTP-bound levels of Cdc42 and Rac1 in *Celsr2*$^{-/-}$ compared to control astrocytes (Figure 2b, e–h; control and mutant: 1.00 ± 0.33 and 2.31 ± 0.11 for total Cdc42, 1 ± 0 and 3.11 ± 0.38 for GTP-bound Cdc42, 1.00 ± 0.14 and 2.27 ± 0.15 for total Rac1, 1 ± 0 and 1.58 ± 0.09 for GTP-bound Rac1, $n = 3$ replicates, $P < 0.05$ or 0.01).

To assess whether blocking Cdc42/Rac1 signaling reverses the phenotypes of *Celsr2*$^{-/-}$ astrocytes, we used the wound scratch assay after addition of inhibitors of Cdc42 (ML141) or Rac1 (NSC23766) and analyzed astrocyte migration 24 h thereafter (Figure 3a, b). In line with the previous report (Etienne-Manneville & Hall, 2001), in control astrocytes, ML141 or NSC23766 significantly slowed down astrocyte migration (Figure 3c, f; sham, control-ML141 and control-NSC23766 in % coverage: 34.6 ± 2.8, 19.6 ± 3.1, and 18.2 ± 3.8; $n = 116$ cells/group, $P < 0.05$, comparisons between sham and controls), limited protrusion extension (Figure 3d, g; sham, control-ML141 and control-NSC23766 in μm: 77.4 ± 2.4, 63.0 ± 2.0 and 58.1 ± 2.0; $n = 116$ cells/group, $P < 0.001$, comparisons between sham and controls; Tables S4 and S5), and impeded protrusion orientation perpendicular to the lesion (Figure 3e, h; 45°–90°: 80/116 in the sham, 63/116 in the control-ML141, 64/116 in the control-NSC23766; $P < 0.05$,

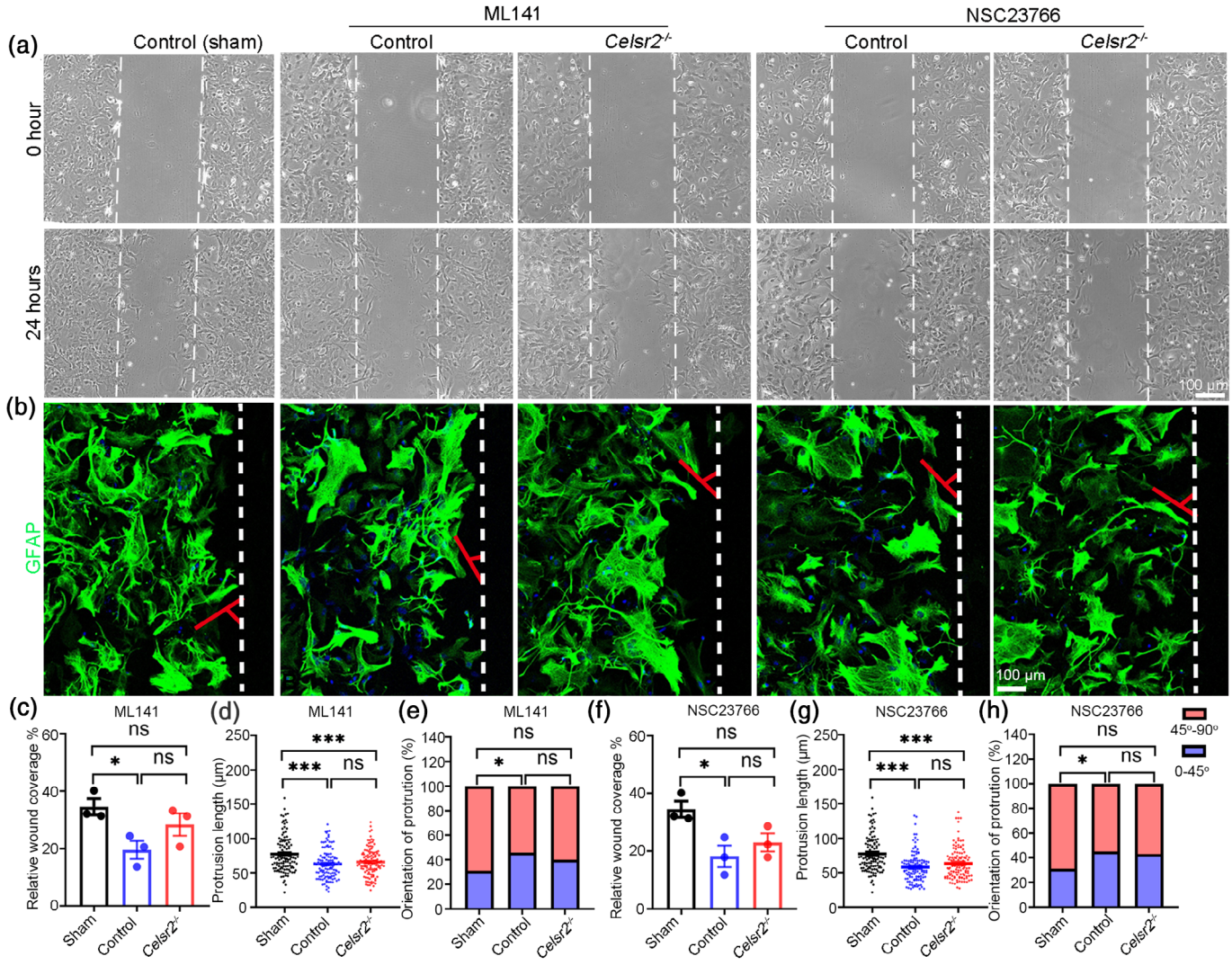

FIGURE 3 Cdc42 and Rac1 inhibitors reverse *Celsr2* inactivation-induced astrocyte motility. a, b. Cultured astrocytes were incubated without inhibitors (sham), with Cdc42 inhibitors (5 μM ML141) or Rac1 inhibitors (50 μM NSC23766) for 24 h, followed with wound scratch. The images show astrocytes and wound regions (dotted lines) at 0 and 24 h (a). Astrocyte protrusions and their orientation (indicated by angles) are visualized by GFAP immunostaining 24 h after scratch (b). c–h. The relative wound coverage (c, f), protrusion length (d, g) and protrusion orientation (e, h) were analyzed in each group. In wildtype astrocytes, ML141 treatment results in decreased lesion coverage, protrusion length and lower numbers of astrocytes with extensions perpendicular to the lesion border. Mutant astrocytes treated with ML141 show no significant differences in the lesion coverage and protrusion orientation compared to wildtype astrocytes with or without inhibitors. Astrocytes treated with NSC23766 show similar changes. Three independent experiments in each group; $n = 116$ cells/group in d, e, g, h. $^*P < 0.05$; $^{***}P < 0.001$; ns, not significant; and one-way analysis of variance with Tukey's multiple comparison test in c, d, f, and g; Chi-square test in e and h.

comparisons between sham and controls). In *Celsr2*$^{-/-}$ mutant astrocytes treated by ML141 or NSC23766, the differences of the relative wound coverage by migrating astrocytes (Figure 3c, f; 28.4 ± 3.9 in the mutant-ML141, 23.0 ± 3.1 in the mutant-NSC23766; $n = 116$ cells/group) and astrocyte protrusion orientation (Figure 3e, h; 45°–90°: 70/116 in the mutant-ML141, 66/116 in the mutant-NSC23766) were diminished compared to the control with or without inhibitors ($P > 0.05$, comparisons of mutants with sham or controls respectively). After the addition of inhibitors, the protrusion length was comparable in control and mutant astrocytes, whereas protrusions remained shorter in mutant compared with control cells in absence of inhibitors(Figure 3d, g; 65.7 ± 1.9 μm in the mutant-ML141, 63.5 ± 2.1 μm in the mutant-NSC23766; $n = 116$ cells, $P < 0.001$, respective comparisons of mutants and shams). These results suggest that Cdc42/Rac1 signaling is a downstream effector of Celsr2 during astrocyte polarization and migration.

3.3 | Inactivating *Celsr2* promotes astrocyte polarization in vivo by enhancing Cdc42/Rac1 signaling after SCI

To further study the role of Celsr2 in vivo, we performed a moderate spinal cord contusion injury at T10 and analyzed astrocyte

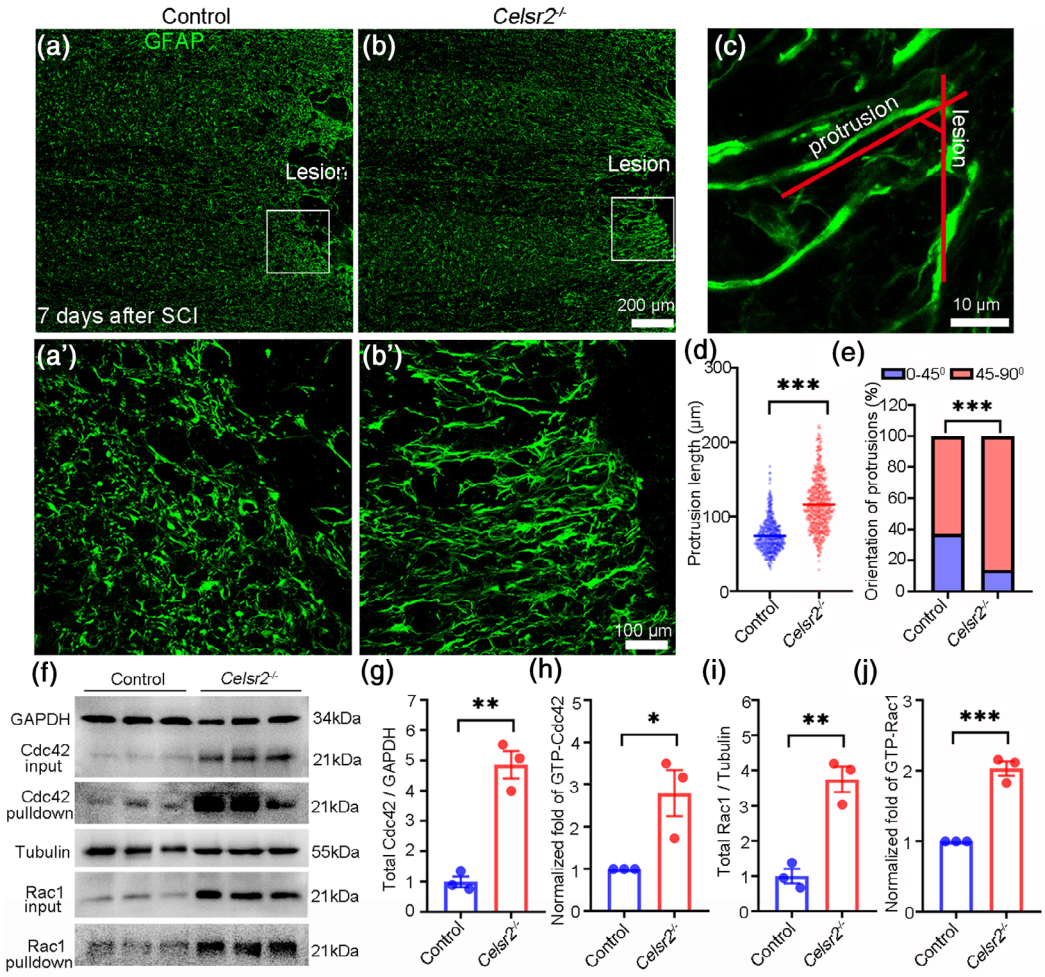

FIGURE 4 *Celsr2* knockout contributes to astrocyte polarization and enhances Cdc42/Rac1 signaling after SCI. a–e. Seven days after contusion SCI, anti-GFAP immunostaining shows reactive and polarized astrocytes surrounding the lesions (a' and b′ from boxed regions in a and b, respectively). In *Celsr2*$^{-/-}$ mice, protrusions are significantly longer (d) and the number of astrocytes with protrusions preferentially perpendicular to the lesion border is increased (e; 45°–90°: 338/537 in the control and 454/529 in the mutant). The measurement is indicated in c. Five animals in each group. f–j: Western blots of the whole protein extracts from spinal samples (T9-T11) 7 days after SCI, or the proteins eluted from GST-bound beads (f). There is a significant increase of total Cdc42 proteins (g), GTP-bound Cdc42 (h), total Rac1 proteins (i), and GTP-bound Rac1 (j) in the mutant compared the control ($n = 3$ animals/group in f–j). *$P < 0.05$; **$P < 0.01$; and ***$P < 0.001$; Student's *t*-test in d, g–j; Chi-square test in e.

morphology around the lesion. GFAP staining of horizontal sections 7 days after SCI disclosed accumulation of reactive astrocytes around lesion sites (Figure 4a, b, a', b′). Within the 250-μm region adjacent to the lesion border, the protrusion length of reactive astrocytes was significantly larger in *Celsr2*$^{-/-}$ compared to control tissue (Figure 4d; control and mutant in μm: 74.3 ± 0.9 and 116.2 ± 1.5, $n = 537$ and 529 cells, $P < 0.001$, $n = 5$ animals in each group; Table S6). In addition, a greater proportion of astrocytes had protrusions preferentially perpendicular to the lesion (indicated in c, 45°–90°) in the mutant than in the control (Figure 4e; control and mutant: 338/537 and 454/529, $P < 0.001$, $n = 5$ animals in each group). These results indicate that, like in vitro, Celsr2 negatively regulates astrocyte polarization.

We then evaluated levels of total and active Cdc42 and Rac1 in spinal cord extracts after SCI. In agreement with in vitro data, both GTP-bound and total Cdc42 and Rac1 protein levels were significantly increased in *Celsr2*$^{-/-}$ compared to control samples (Figure 4f-j); control and mutant: 1.00 ± 0.18 and 4.86 ± 0.46 for total Cdc42, 1 ± 0 and 2.80 ± 0.54 for GTP-bound Cdc42, 1.00 ± 0.21 and 3.75 ± 0.36 for total Rac1, 1 ± 0 and 2.03 ± 0.10 for GTP-bound Rac1 ($n = 3$ replicates; $P < 0.01$, 0.05, 0.01, and 0.001, respectively).

3.4 | *Celsr2* inactivation improves healing of SCI lesions

After SCI, polarized astrocytes fill the lesion cavity and contribute to neural repair (Assinck et al., 2017; Renault-Mihara et al., 2011). We first investigated the effect of *Celsr2* inactivation on healing of a small lesion made by a hemisection. Eight weeks after injury, serial

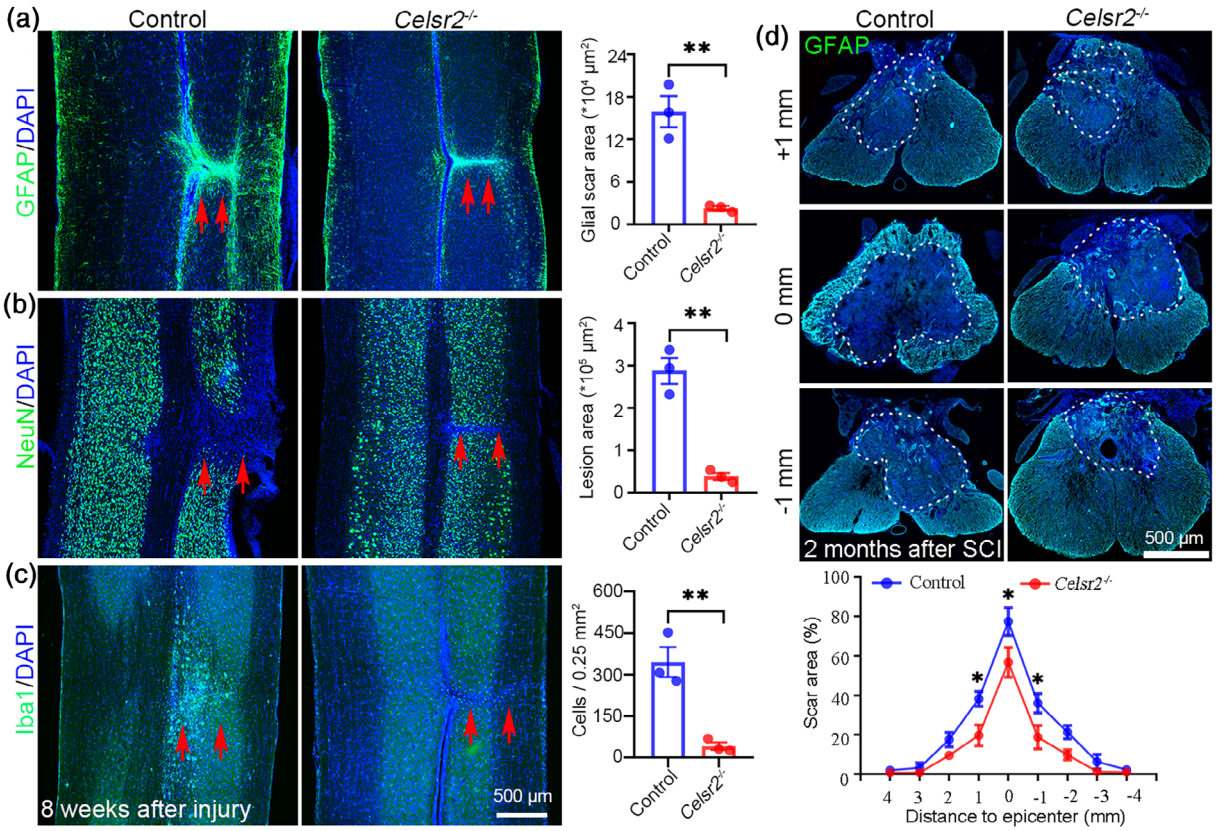

FIGURE 5 *Celsr2*$^{-/-}$ animals have improved wound healing after SCI. a–c: Eight weeks after hemisection, horizontal sections are immunostained for GFAP (a), NeuN (b) and Iba1 (c). Lesion areas are indicated by red arrows. Note the significant decrease of GFAP-positive glia scar area, neuron-depleted lesion area, and Iba1-positive microglia in the mutant compared to the control. $^{**}P < 0.01$; $n = 3$ animals in each group; Student's *t*-test. d. Transverse sections immunolabeled for GFAP at different distances from injury sites, 2 months after contusion SCI; lesion cavities are visualized by astrocyte surroundings (dot circles), showing the significant decreases at +1 mm, 0 mm, −1 mm, in mutants compared to controls. $^{*}P < 0.05$; $n = 5$ animals in each group; Two-way ANOVA with Bonferroni's *post hoc* correction.

horizontal sections were stained with anti-GFAP, -NeuN and -Iba1 antibodies (Figure 5a–c). Strongly reactive astrocytes covered the lesion sites in both genotypes, while the astrocyte-covered area was markedly smaller in *Celsr2*$^{-/-}$ compared to control sections (Figure 5a; control and mutant in 10^4 μm^2: 15.9 ± 2.2 and 2.3 ± 0.3, $P < 0.01$). The local lesion area identified by the absence of NeuN-positive neurons was significantly decreased in the mutant (Figure 5b; control and mutant in 10^5 μm^2: 2.88 ± 0.31 and 0.38 ± 0.08, $P < 0.01$). Furthermore, less reactive microglia were scattered in the lesions in the mutant compared to the control (Figure 5c; control and mutant in 0.25 mm^2: 345 ± 54 and 41 ± 13 cells; $P < 0.01$).

The contribution of *Celsr2* inactivation to lesion healing was then verified using a more severe model of SCI. We performed moderate contusions at T10 and collected spinal cords after 2 months. In transverse sections, the lesion cavities were visualized by anti-GFAP immunostaining, showing glial scars gradually shrinking from the epicenter to the rostral and caudal levels in both genotypes (Figure 5d). In *Celsr2*$^{-/-}$ samples, lesion areas were significantly smaller than in controls at 1 mm (19.77 ± 5.34% vs. 38.20 ± 3.76%), 0 mm (56.74 ± 7.57% vs. 77.42 ± 7.08%) and −1 mm (18.83 ± 5.98% vs. 36.06 ± 4.94%) from the injury center (Figure 5d; $P < 0.05$). Thus, increased astrocyte motility in *Celsr2*$^{-/-}$ mutant correlates with improved SCI lesion healing.

3.5 | *Celsr2*$^{-/-}$ mutants have better functional recovery after SCI

To evaluate the effect of Celsr2 inactivation on functional recovery, we assessed mouse hindlimb movement after a moderate contusion at T10, using BMS scores. All mice showed complete hindlimb paralysis 1 day after injury, with a BMS score of 0, followed by some spontaneous recovery in both groups (Figure 6a). Starting from day 35, BMS scores were significantly higher in *Celsr2*$^{-/-}$ mutants than in control animals (Figure 6a; control and mutant: 3.1 ± 0.4 and 4.7 ± 0.2 at day 35, 3.4 ± 0.3 and 5.0 ± 0.2 at day 42, 3.7 ± 0.3 and 5.2 ± 0.2 at day 49, 3.8 ± 0.3 and 5.2 ± 0.2 at day 56; $P < 0.05$ at day 56 and $P < 0.01$ at rest timepoints). In Catwalk tests, the number of wrong steps of the hindlimb was reduced in *Celsr2*$^{-/-}$ mutants compared with controls (Figure 6b); the regularity index was improved (Figure 6c; control and mutant: 33.8 ± 5.0 and 64.7 ± 6.8, $P < 0.01$, $n = 7$, Student's *t*-test); the maximal contact areas of hindpaws were

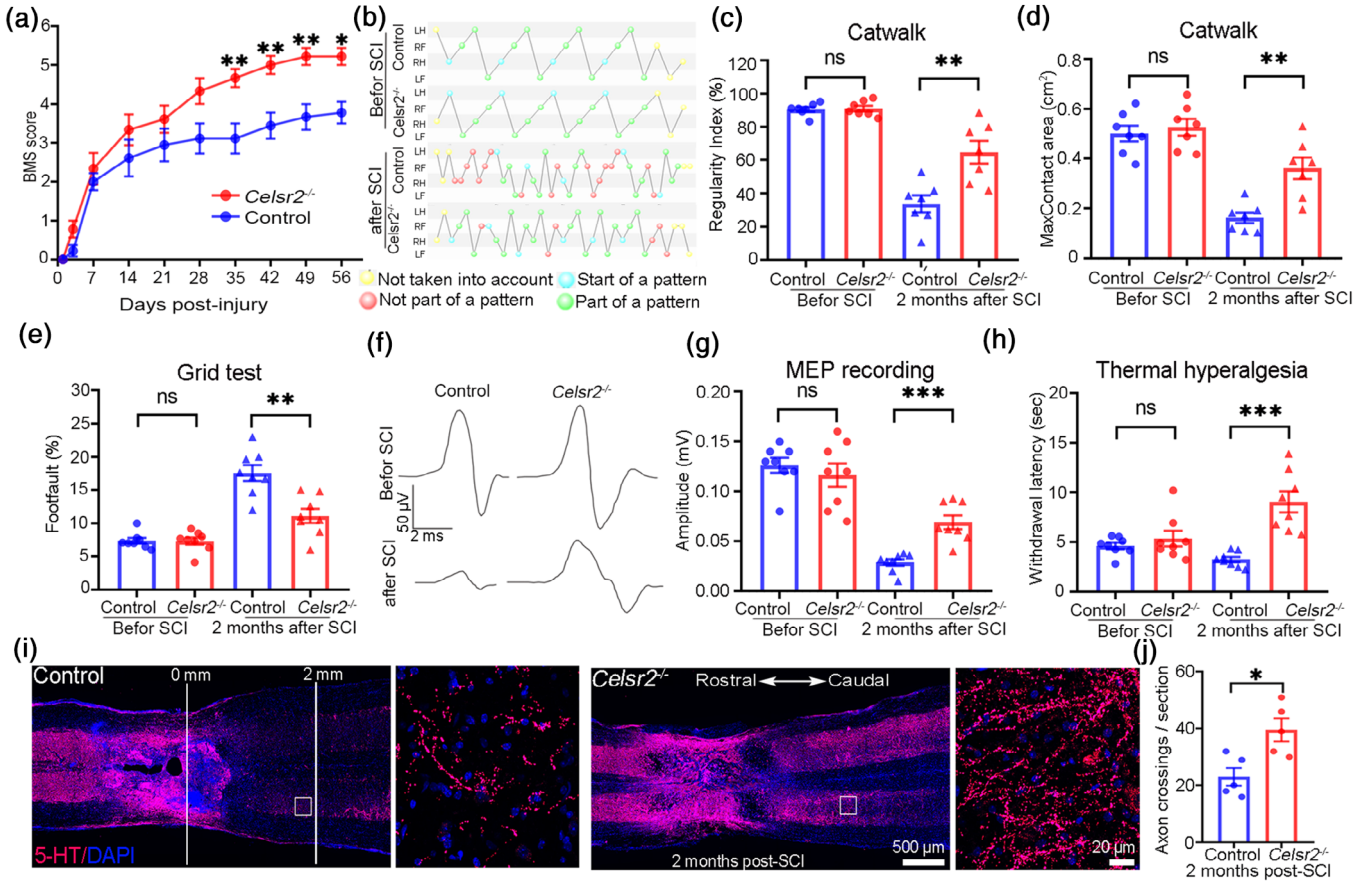

FIGURE 6 *Celsr2*$^{-/-}$ mice exhibit improved functional recovery and axon regeneration after SCI. a. Elevation of BMS scores shows significantly higher at day 35, 42, 49, and 56 after SCI in the *Celsr2*$^{-/-}$. Nine animals in each group. b–d. In Catwalk test at 2 months after SCI (b, $n = 7$ mice in each group), the Regularity Index and the Max Contact areas of hindpaws are significantly increased in the mutant, whereas they are comparable in both groups before SCI (c, d). Dots in b. yellow, gaits not considered; blue, starting gaits; green, normal gaits; red, wrong gaits. e. Grid tests show a decrease of the footfault percentage in *Celsr2*$^{-/-}$ mice 2 months after SCI, but no differences before injury ($n = 8$ mice in each group). f, g. MEP recording shows a significant increase of amplitude in the mutant, but no differences before injury ($n = 8$ animals in each group). h. In thermal hyperemesis, the withdraw latency is increased in the mutant, but no differences before SCI ($n = 8$ animals in each group). i, j. Anti-5-HT immunostaining of horizontal spinal sections discloses serotoninergic fibers 2 months after SCI (i; horizontal lines indicate caudal distances to the lesion epicenter panel). Enlarged images (two lower panels) show more serotoninergic fibers in the caudal region (boxed in two upper panels) in the mutant. At the panel of 2 mm caudal to the lesion, axon crossings are significantly increased in the *Celsr2*$^{-/-}$ compared to the control (j), five animals in each group. *$P < 0.05$; **$P < 0.01$; and ***$P < 0.001$; and ns, not significant. Two-way ANOVA with Bonferroni's *post hoc* correction in a; Student's *t*-test in c, d, e, g, h, and j.

increased in *Celsr2*$^{-/-}$ mice at 2 months after SCI (Figure 6d; control and mutant: 0.16 ± 0.02 and 0.36 ± 0.04, $P < 0.01$). These parameters in Catwalk tests did not differ in the two groups prior to injury (Figure 6b–d, $P > 0.05$). Similarly, the footslip scores in grid tests were similar in both groups before injury (Figure 6e), but significantly lower in the mutant than in the control at 2 months after SCI (Figure 6e; 11.1 ± 1.1% vs.17.6 ± 1.2%, $P < 0.01$). Upon stimulation of motor cortex, the amplitude of MEP in the gastrocnemius was similar prior to injury, but significantly higher in the mutant than in the control (Figure 6f, g; 0.07 ± 0.01 mV vs. 0.03 ± 0.00 mV, $P < 0.001$) 2 months after injury. We also used laser stimulation of hindpaws to detect thermal hyperalgesia. The withdrawal thresholds were comparable in both groups before SCI, and significantly increased in the *Celsr2*$^{-/-}$ compared to the control at 2 months after SCI (Figure 6h; 9.06 ± 1.06 vs. 3.26 ± 0.27, $P < 0.001$).

We also performed magnetic resonance imaging (MRI) scanning on live animals to measure T2WI and diffusion tensor imaging (DTI) 2 months after contusion SCI (Figure S3A). Fractional anisotropy (FA) values, which positively correlate with axon density (Lehmann et al., 2010), were significantly increased at +3 mm, +2 mm, −2 mm, −3 mm to injury centers in *Celsr2*$^{-/-}$ mutants compared to control mice (Figure S3B; mutant vs. control: 0.43 ± 0.03 vs. 0.33 ± 0.03 at +3 mm, $P < 0.05$; 0.36 ± 0.02 vs. 0.26 ± 0.03 at +2 mm, $P < 0.05$; 0.35 ± 0.02 vs. 0.25 ± 0.02 at −2 mm $P < 0.05$; 0.41 ± 0.03 vs. 0.31 ± 0.02 at −3 mm, $P < 0.05$). Radial diffusivity (RD) values, reflecting axon demyelination after SCI (Aung et al., 2013), were significantly decreased in *Celsr2*$^{-/-}$ mutant at +1 mm, 0 mm, −1 mm, −2 mm (Figure S3C; mutant vs. control: 3.53 ± 0.37 vs. 5.23 ± 0.38 at +1 mm, $P < 0.05$; 4.61 ± 0.55 vs. 6.45 ± 0.49 at 0 mm, $P < 0.01$; 3.73 ± 0.50 vs. 5.42 ± 0.44 at −1 mm, $P < 0.05$; 3.08 ± 0.34 vs. 4.56

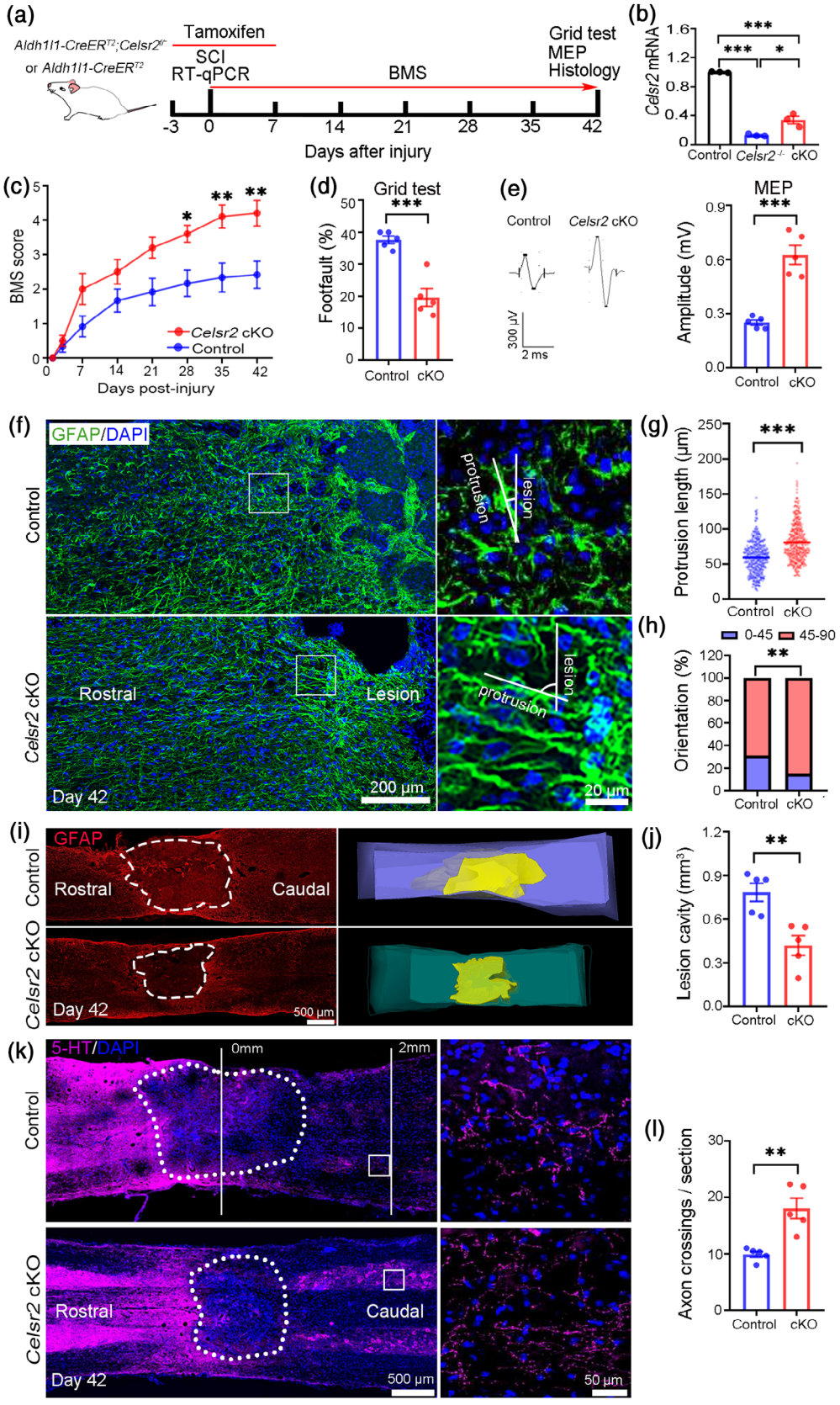

FIGURE 7 Legend on next page.

± 0.41 at −2 mm, $P < 0.05$). Statistical analysis showed that the lesion areas were dramatically reduced in the *Celsr2*$^{-/-}$ compared to the control (Figure S3D; mutant vs. control: 21.73 ± 2.61 vs. 39.40 ± 4.66, at +1 mm, $P < 0.05$; 43.26 ± 4.27 vs. 62.65 ± 6.42 at 0 mm, $P < 0.05$; 22.76 ± 4.08 vs. 41.79 ± 4.36 at −1 mm, $P < 0.05$).

After MRI scanning, we collected spinal cords and estimated regenerating fibers by visualizing serotoninergic fibers, as reported before (Ghosh & Pearse, 2014). In horizontal sections, large 5-HT-positive fibers were identified in segments rostral to the injury sites, and some bundled together around lesion cavities, similarly in both groups (Figure 6i). In contrast, in more caudal spinal segments, more serotoninergic fibers were visualized in the mutant than in controls (Figure 6i), as confirmed by statistical analysis (Figure 6j; mutant vs. control: 39.60 ± 4.01 vs. 23.00 ± 3.16 fibers/section, $P < 0.05$).

3.6 | Conditional knockout of *Celsr2* in astrocytes contributes to neural repair and functional recovery after SCI

To further confirm the role of Celsr2 in spinal astrocytes for neural repair, we used *Aldh1l1-CreER*^{T2}; *Celsr2*$^{f/-}$ mice (*Celsr2* cKO), in which *Celsr2* was specifically inactivated in astrocytes upon tamoxifen induction (Hu et al., 2020). Animals were subjected to intraperitoneal injection of tamoxifen for 10 consecutive days, 3 days before and 7 days after SCI (Figure 7a). RT-qPCR showed a significant knockdown of *Celsr2* mRNA in spinal samples after tamoxifen induction (Figure 7b), although the level of *Celsr2* mRNA was still higher in *Celsr2* cKO sample than that in the *Celsr2*$^{-/-}$ (normalized to control: 12.8 ± 0.9% in *Celsr2*$^{-/-}$ and 33.8 ± 5.3% in *Celsr2* cKO, $P < 0.05$). Nevertheless, like *Celsr2*$^{-/-}$ mice, *Celsr2* cKO animals had a better functional recovery than control mice, as indicated in BMS scores (Figure 7c), by the decrease of footfault percentage in grid tests (Figure 7d; control and cKO: 37.6 ± 1.2% and 19.6 ± 2.8%, $P < 0.001$) and by the elevated amplitude of MEP (Figure 7e; control and cKO: 0.25 ± 0.01 mV and 0.63 ± 0.06 mV, $P < 0.001$). In the lesion border 42 days after SCI, astrocytes showed significantly longer protrusions in cKO mutants compared to controls (Figure 7f, g; control and cKO in μm: 59.5 ± 1.0 and 80.8 ± 1.2, $P < 0.001$, $n = 478$ and 469 cells, respectively), with more protrusions preferentially oriented perpendicular to the lesion border (Figure 7h; 45°–90° angle: 254/369 in control and 292/343 in cKO, $P < 0.01$). Compared to control mice, 42 days after SCI, the volume of lesion cavity was significantly decreased (Figure 7i, j; control and cKO in mm^3: 0.78 ± 0.06 and 0.42 ± 0.07, $P < 0.01$), and more serotoninergic fibers were visible in the region caudal to the lesion site (Figure 7k, l; control and cKO: 9.9 ± 0.5 and18.1 ± 1.8 crossings/section at 2 mm caudal to lesion, $P < 0.01$). These findings suggest that *Celsr2* downregulation in astrocytes efficiently reduces lesion size, facilitates axon regeneration, and improves functional recovery after SCI.

3.7 | Inhibiting Cdc42/Rac1 activity compromises astrocyte polarization and the improvement of neural repair and functional recovery in *Celsr2*$^{-/-}$ mice with SCI

To further identify whether Cdc42 and Rac1 are the downstream effectors of Celsr2 in vivo, *Celsr2*$^{-/-}$ mice after SCI were subjected to intraperitoneal injection of Cdc42 and Rac1 inhibitors once a day for 14 consecutive days (Figure 8a). At day 7, the protein levels of total and GTP-bound Cdc42 and Rac1 in spinal samples were significantly downregulated in *Celsr2*$^{-/-}$ mutants with inhibitor treatment compared to those without inhibitor treatment (Figure S4). Inhibitor administration remarkably reversed the functional improvement in *Celsr2*$^{-/-}$ mutants as shown in BMS scores (Figure 8b), grid tests (Figure 8c; percentage of footfault: control, *Celsr2*$^{-/-}$ and *Celsr2*$^{-/-}$ + inhibitors: 43.00 ± 3.53%, 23.00 ± 3.17% and 44.33 ± 4.69%; $n = 6$, $P < 0.01$ in the comparisons of *Celsr2*$^{-/-}$ with control or *Celsr2*$^{-/-}$ + inhibitors) and MEP recording (Figure 8d; amplitude in control, *Celsr2*$^{-/-}$ and *Celsr2*$^{-/-}$ + inhibitors: 0.17 ± 0.02 mV, 0.32 ± 0.03 mV and 0.13 ± 0.02 mV; $n = 6$, $P < 0.01$ or 0.001 in the comparisons of *Celsr2*$^{-/-}$ with control or *Celsr2*$^{-/-}$ + inhibitors respectively). In *Celsr2*$^{-/-}$ mice, the enhanced polarization of reactive

FIGURE 7 Conditional knockout of *Celsr2* in astrocytes contributes to neural repair and functional recovery after SCI. a, b: Inactivation of *Celsr2* is induced by intraperitoneal injection of tamoxifen and the main procedure is indicated (a). Validation is examined using RT-qPCR of spinal samples (b). *Celsr2*$^{-/-}$ samples are used as negative control. *$P < 0.05$; ***$P < 0.001$; Student's *t*-test, $n = 3$ animals in each group. c–e: Improved recovery in *Celsr2* cKO animals are indicated in elevated BMS scores (c), the decrease of footfault percentage in grid tests (d, $n = 5$), and the increased amplitude of MEP recording (e, $n = 5$). *$P < 0.05$; **$P < 0.01$; and ***$P < 0.001$; Two-way ANOVA with Bonferroni's post hoc correction in c, Student's *t*-test in d and e. f–h: Horizontal sections are immunostained for GFAP (green) 42 days after SCI, and astrocytes in lesion border are analyzed indicated in right panels (f). In *Celsr2* cKO mice, average protrusion length of reactive astrocytes is significantly longer (g, $n = 478$ and 469 cells in control and cKO, respectively), and the increased percentage of astrocytes show the angle of protrusion axis and lesion border in 45°–90° (h; 69% in control and 85% in cKO). **$P < 0.01$; ***$P < 0.001$; Student's *t*-test in g and Chi-Square in h, five animals in each group. i, j. Horizontal sections are immunostained for GFAP (red) and followed with reconstruction (right panels) 42 days after SCI (i). Qualification shows a decrease of lesion volume in *Celsr2* cKO mice (j, $n = 5$). Dotted circles indicate lesion areas. **, $P < 0.01$; Student's *t*-test. k, l: Anti-5-HT immunostaining (red) shows serotoninergic fibers in horizontal sections 42 days after SCI, and examples of axons in caudal regions are shown in right panels from rectangle regions in left panels respectively (k). Dotted circles indicate lesion areas, and perpendicular lines show the distance to lesion epicenter as the reference for axon crossing count. Qualification analysis shows a significant increase of axon crossings at 2 mm caudal to the lesion epicenter in *Celsr2* cKO mice (l, $n = 5$). **$P < 0.01$; Student's *t*-test.

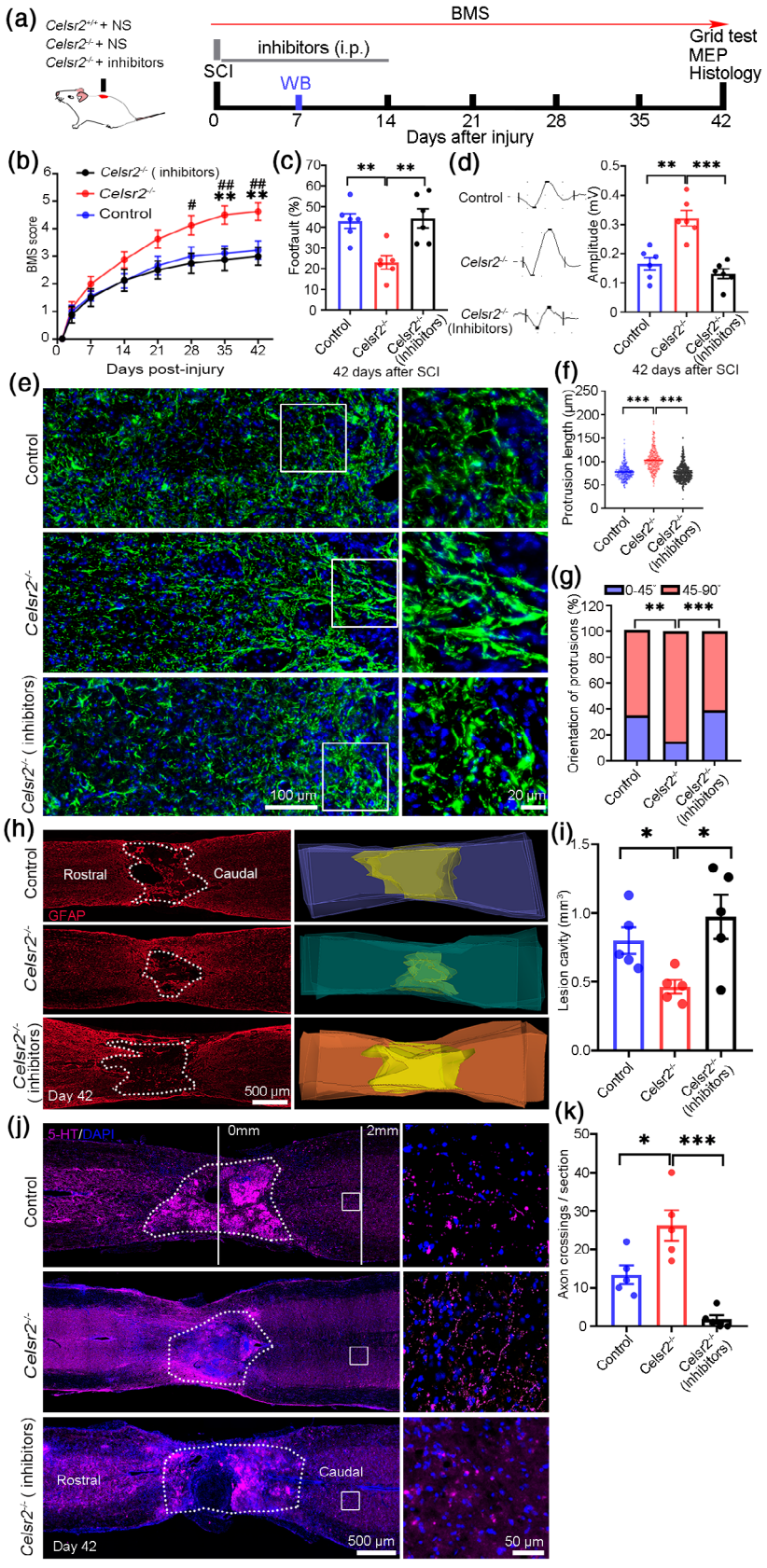

FIGURE 8 Administration of Cdc42 and Rac1 inhibitors compromise the improvement of neural repair and functional recovery in *Celsr2*$^{-/-}$ mice after SCI. a. Illustration of the experimental procedure. b–d. In the *Celsr2*$^{-/-}$, the BMS scores are significantly higher (b; $n = 8$, Two-way ANOVA with Bonferroni's post-hoc correction) and the footfault percentage is decreased (c; $n = 6$, one-way ANOVA analysis of variance with Tukey's multiple comparison) compared to the control or the *Celsr2*$^{-/-}$ + inhibitors. The amplitude of MEP recording is bigger in the *Celsr2*$^{-/-}$ compared to the control or the *Celsr2*$^{-/-}$ + inhibitors (d; $n = 6$, one-way ANOVA analysis of variance with Tukey's multiple comparison). * and # indicate the comparisons of the *Celsr2*$^{-/-}$ with the control and the *Celsr2*$^{-/-}$ + inhibitors, respectively. *P < 0.05; **P < 0.0 1; ***P < 0.001; #P < 0.05; and ##P < 0.01. e–g: Horizontal spinal sections are immunostained for GFAP at day 42 after SCI (e). Compared to the control and the *Celsr2*$^{-/-}$ + inhibitors, the average protrusion length of reactive astrocytes is longer and the cells with the angle of protrusion axis and lesion border in 45°–90°are significantly increased in the *Celsr2*$^{-/-}$ (f, g). Images in the right panel are from the selected regions of lesion borders in the left panel, respectively. In the control, the *Celsr2*$^{-/-}$ and *Celsr2*$^{-/-}$ + inhibitors: $n = 461$, 419, and 445 cells in f, and 329/500, 423/500 and 305/500 in g. **P < 0.01; ***P < 0.001; one-way ANOVA analysis of variance with Tukey's multiple comparison in f and Chi-Square in g, five animals in each group. h, i: At day 42 after SCI, lesion cavities (dotted circles, left panel) are analyzed from anti-GFAP immunostained spinal sections and reconstructed by the Imaris software (right panel) in three groups (h). Qualification shows a decrease of lesion volume in the *Celsr2*$^{-/-}$ compared to the control and the *Celsr2*$^{-/-}$ + inhibitors (i). *, P < 0.05; $n = 5$ in each group, one-way ANOVA analysis of variance with Tukey's multiple comparison. j, k. Anti-5-HT immunostaining shows serotoninergic fibers in horizontal spinal sections 42 days after SCI, and examples of axons in the caudal regions are shown in the right panel from rectangle regions in the left panel respectively (j). Dotted circles indicate lesion areas, and perpendicular lines show the distance to the lesion epicenter as the reference for axon crossing count. Qualification analysis shows more axon crossings at 2 mm caudal to the lesion epicenter in the *Celsr2*$^{-/-}$ compared to the control and the *Celsr2*$^{-/-}$ + inhibitors respectively (k). *P < 0.05; ***P < 0.001; $n = 5$, one-way ANOVA analysis of variance with Tukey's multiple comparison.

astrocytes surrounding the lesion was also diminished by inhibiting Cdc42 and Rac1 activity after SCI (Figure 8e). At day 42 after SCI, the average protrusion length of reactive astrocyte was 77.26 ± 0.68 μm in the control, 103.50 ± 1.20 μm in the *Celsr2*$^{-/-}$ and 75.95 ± 0.81 μm in the *Celsr2*$^{-/-}$ + inhibitors (Figure 8f; P < 0.001, comparisons of *Celsr2*$^{-/-}$ with control or *Celsr2*$^{-/-}$ + inhibitors respectively,

$n = 461$, 416 and 445 cells, five animals in each group). The preferential orientation of astrocyte protrusion perpendicular to the lesion border in *Celsr2*$^{-/-}$ mutants was reversed after the treatment of the inhibitors (Figure 8g; 45°–90° angle: 329/500 in the control, 423/500 in the *Celsr2*$^{-/-}$ and 305/500 in the *Celsr2*$^{-/-}$ + inhibitors; $P < 0.01$ or 0.001 in the comparisons of *Celsr2*$^{-/-}$ with control or

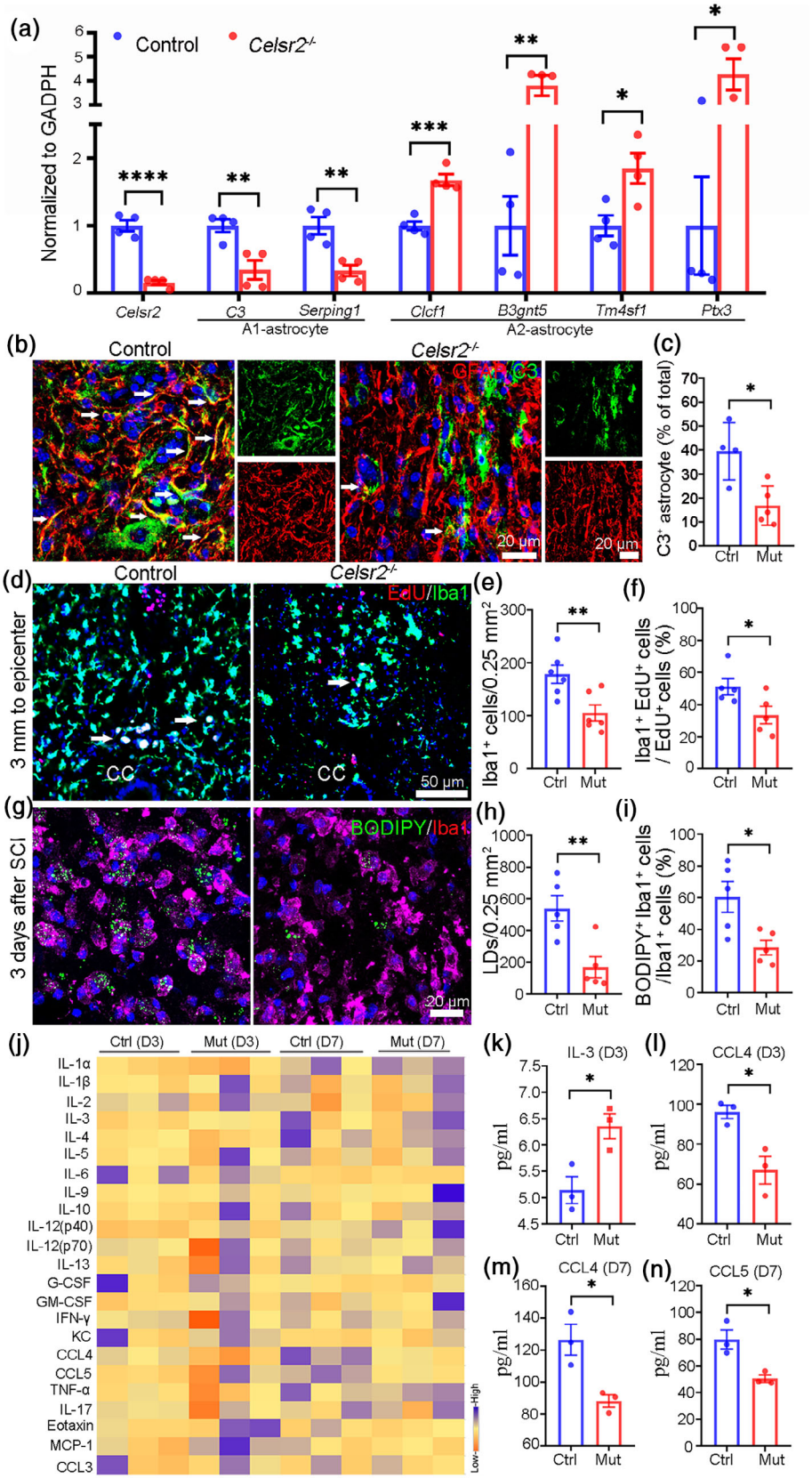

FIGURE 9 *Celsr2* inactivation promotes phenotype switch of reactive astrocytes and alleviates neuroinflammation after SCI. a: RT-qPCR quantification of *Celsr2*, *C3*, and *Serping1* (A1 phenotype), and *Clcf1*, *B3gnt5*, *Tm4sf1*, and *Ptx3* (A2 phenotype) transcripts in cultured spinal cord astrocytes. The mRNA levels are normalized to that of *GAPDH*. *$P < 0.05$; **$P < 0.01$; ***$P < 0.001$; and ****$P < 0.0001$; Student's *t*-test, $n = 4$ independent experiments in each group. b, c: At 7 days after SCI, spinal sections were prepared for anti-GFAP (red) and -C3 (green) double immunostaining (b). Quantitative analysis shows the percentage of C3-expressed astrocytes is lower in the *Celsr2*$^{-/-}$ (Mut) compared to the control (Ctrl) (c). *$P < 0.05$; Student's *t*-test, $n = 4$ and five animals in the control and the *Celsr2*$^{-/-}$, respectively. DAPI (blue) counterstained nuclei. d–f. In spinal transverse sections 2 months after SCI, EdU (red) and Iba1 (green) immunostaining shows proliferating cells and microglia (d). Quantitative analysis indicates the decrease of Iba1-positive cell density (e) and the percentage of double labeled cells (arrows) to total EdU-positive cells in the *Celsr2*$^{-/-}$ (Mut) compared to the control (Ctrl) (f). *$P < 0.05$; **$P < 0.01$; Student's *t*-test, $n = 5$ animals in each group. DAPI (blue) counterstained nuclei; cc, central canal. g–i. BODIPY (green) and anti-Iba1 staining (red) of spinal sections at the lesion level 3 and 7 days after SCI (g) show a decrease of lipid droplets (LDs) in the *Celsr2*$^{-/-}$ compared to the control (h). The percentage of LDs-containing Iba1-positive cells is lower in the mutant at day 3 (i). *$P < 0.05$; **$P < 0.01$; ns, not significant; Student's *t*-test, $n = 5$ animals in each group. j–n: The heatmap of the Bioplex analysis presents the relative expression of 23 cytokines in spinal samples in two groups at day 3 (D3) and 7 (D7) after SCI (j). Quantitative analysis shows an increase of IL-3 and a decrease of CCL4 at day 3 in the mutant (k, l), and a decrease of CCL4 and CCL5 in the mutant at day 7 (m, n). *$P < 0.05$; Student's *t*-test, $n = 3$ animals in each group.

Celsr2$^{-/-}$ + inhibitors respectively, five animals in each groups). Additionally, inhibitor treatment significantly compromised the improvement of lesion healing and axon regeneration in *Celsr2*$^{-/-}$ mice after SCI (Figure 8h, j). At day 42 after SCI, the lesion cavity was significantly decreased in the *Celsr2*$^{-/-}$ compared to the control or the *Celsr2*$^{-/-}$ + inhibitors (Figure 8i; control, *Celsr2*$^{-/-}$ and *Celsr2*$^{-/-}$ + inhibitors in mm^3: 0.80 ± 0.10, 0.46 ± 0.05 and 0.97 ± 0.16, $n = 5$, $P < 0.05$ in the comparisons of *Celsr2*$^{-/-}$ with control or *Celsr2*$^{-/-}$ + inhibitors). More serotoninergic fibers were visible in the region caudal to the lesion center in the *Celsr2*$^{-/-}$ compared to the control or the *Celsr2*$^{-/-}$ + inhibitors (Figure 8k; crossing axons in control, *Celsr2*$^{-/-}$ and *Celsr2*$^{-/-}$ + inhibitors: 13.40 ± 2.44, 26.20 ± 4.02 and 1.80 ± 1.11, $n = 5$, $P < 0.05$ or 0.001 in the comparisons of *Celsr2*$^{-/-}$ with control or *Celsr2*$^{-/-}$ + inhibitors respectively). These findings suggest that Cdc42 and Rac1 are the downstream partners of Celsr2 during astrocyte polarization, lesion healing and axonal regeneration.

3.8 | *Celsr2* inactivation promotes phenotype switch of reactive astrocytes to alleviate neuroinflammation

Reactive astrocytes upon injury undergo complex morphological, molecular and functional changes (Escartin et al., 2021). In the early study, astrocytes were described as A1 and A2 phenotypes based on their gene expression, secreted cytokines and function (Liddelow et al., 2017). Using a similar classification, we further investigated the effect of *Celsr2* inactivation on astrocyte phenotype. Cultured spinal astrocytes were stimulated by the macrophage-conditioned medium for 24 h and then their mRNA was collected for RT-qPCR. In *Celsr2*$^{-/-}$ samples, there were much lower levels of *Celsr2* (control and *Celsr2*$^{-/-}$: 1.00 ± 0.08 and 0.16 ± 0.04, $P < 0.0001$), A1-phenotype genes *C3* (control and *Celsr2*$^{-/-}$: 1.00 ± 0.10 and 0.35 ± 0.14, $P < 0.01$) and *Serping1* (control and *Celsr2*$^{-/-}$: 1.00 ± 0.13 and 0.34 ± 0.08, $P < 0.01$), and higher levels of A2-pehnotype genes *Clcf1* (control and *Celsr2*$^{-/-}$: 1.00 ± 0.06 and 1.68 ± 0.08, $P < 0.001$), *B3gnt5* (control and *Celsr2*$^{-/-}$: 1.00 ± 0.44 and 3.81 ± 0.43, $P < 0.01$), *Tm4sf1* (control and *Celsr2*$^{-/-}$: 1.00 ± 0.15 and 1.85 ± 0.23, $P < 0.05$) and *Ptx3* (control and *Celsr2*$^{-/-}$: 1.00 ± 0.73 and 4.27 ± 0.65, $P < 0.05$), compared to wildtype (control) samples (Figure 9a). In injured spinal sections, anti-C3 immunostaining also showed the percentage of C3-expressed astrocytes was significantly higher in the control compared to the *Celsr2*$^{-/-}$ (Figure 9b, c; control and *Celsr2*$^{-/-}$: 39.50 ± 6.00 and 16.80 ± 3.67, $P < 0.05$).

After injury, microglial cells and astrocytes interact closely, and activation of astrocytes upon SCI may influence microglial activation and neuroinflammation (Jo et al., 2017). Two months after spinal cord contusion, microglial proliferation was studied by Iba1 and EdU double immunostaining. The density of Iba1-positive cells and the percentage of double-labeled cells to total EdU-positive cells were significantly decreased in mutant compared to control spinal cords (Figure 9d–f; control and *Celsr2*$^{-/-}$: 178.3 ± 17.1 and 105.5 ± 14.9 cells/0.25mm^2, 51.3 ± 5.1 and 33.4 ± 5.5%, $P < 0.01$ and 0.05).

To further evaluate microglial function, we performed BODIPY staining to visualize lipid droplets in microglia, 3 days after contusion SCI, and found a significant decrease of lipid droplets in the injured areas of mutant versus control samples (Figure 9g, h; control and *Celsr2*$^{-/-}$ in 0.25 mm^2: 538.8 ± 80.1 and 168.6 ± 66.6, $P < 0.01$). The proportion of lipid droplet-containing microglia to total Iba1-positive microglia was lower in the mutant group than the control at day 3 (Figure 9i; control and *Celsr2*$^{-/-}$: 60.5 ± 9.7% and 28.4 ± 4.5%, $P < 0.05$).

We also collected injured spinal samples 3 days and 7 days after contusion, and measured cytokine levels, using the bioplex assay (Figure 9j). Compared to controls, an increase of IL-3 and a decrease of CCL4 were found in the *Celsr2*$^{-/-}$ at day 3 (Figure 9k, l; control and *Celsr2*$^{-/-}$ in pg/ml: 5.15 ± 0.26 and 6.36 ± 0.24 for IL-3, 96.10 ± 3.31 and 66.99 ± 6.88, $P < 0.05$), while both CCL4 and CCL5 was significantly decreased in the mutant (Figure 9m, n; control and *Celsr2*$^{-/-}$ in pg/ml: 126.50 ± 9.62 and 88.22 ± 3.83 for CCL4, 79.82 ± 7.16 and 50.56 ± 2.78 for CCL5, $P < 0.05$).

4 | DISCUSSION

In the present work, we uncover the previously unexpected role of Celsr2 in reactive astrocytes, and provide evidence that *Celsr2* inactivation enhances spinal astrocyte polarization and migration, and promotes the phenotype switch of reactive astrocytes, which changes contribute to lesion healing, axonal regeneration, and functional recovery after SCI. Firstly, *Celsr2* is highly expressed in spinal astrocytes in intact and injured spinal cords. Secondly, *Celsr2* inactivation promotes astrocyte protrusion extension with a preferential orientation towards the lesion in vitro as well as in vivo. Thirdly, after SCI, *Celsr2*$^{-/-}$ and *Celsr2* cKO mice have smaller lesion cavity and increased fibers in the caudal to the lesion compared to control mice. Fourthly, *Celsr2*$^{-/-}$ and *Celsr2* cKO mice show similarly improved functional recovery after SCI. Fifthly, the total and active Rac1 and Cdc42 protein levels are upregulated in cultured astrocytes and spinal samples after SCI in *Celsr2* mutants and inhibiting their activity reverses phenotypes of cultured astrocytes with *Celsr2* mutation. Finally, cultured spinal astrocytes from *Celsr2*$^{-/-}$ mice present A2 phenotype and the neuroinflammation response is alleviated in *Celsr2*$^{-/-}$ injured spinal cords.

Astrocytes play crucial roles in neural function and plasticity (Freeman, 2010). In areas surrounding SCI lesions, astrocytes undergo morphological, molecular, and functional changes (Karimi-Abdolrezaee & Billakanti, 2012). Increasing evidence indicates that reactive gliosis is critical for neural repair, with both beneficial and detrimental roles (Burda & Sofroniew, 2014). In the acute phase of SCI, traumatic injury induces astrocyte polarization, characterized by the elongation of reactive astrocytes with the emission of protrusions, and the orientation of these protrusions towards the lesion. These polarized astrocytes migrate towards and around lesions to limit the infiltration by inflammatory cells (Okada et al., 2006). Wound scratch is a favored in vitro model to evaluate the factors

influencing astrocyte polarity. In our spinal astrocyte culture, reactive astrocytes induced by scratching displayed longer protrusions, with more perpendicular direction relative to lesion borders, in *Celsr2* mutants compared to control samples. A similar phenomenon is found around lesions in vivo after SCI. Upon stimulation by the macrophage-conditioned medium, *Celsr2*$^{-/-}$ astrocyte migration was substantially increased compared to wildtype. Calcium influx is an indicator for the changes of cell motility, and a higher calcium release upon ATP stimulation was also identified in cultured mutant astrocytes. These results indicate that Celsr2 is a negative regulator involved in astrocyte morphological polarization and migration in response to injury.

Small GTPase Cdc42 and Rac1 are critical regulators of astrocyte polarization. Cdc42 initiates the formation of protrusions by recruiting and activating a cytoplasmic mPar6/PKCζ complex, while Rac1 activity is essential for the extension of the protrusions (Etienne-Manneville & Hall, 2001). Integrins and Scrib control Cdc42 localization and activity, which subsequently influence astrocyte polarization (Etienne-Manneville & Hall, 2001; Osmani et al., 2006). Genetic inactivation of Cdc42 resulted in impaired recruitment and migration of astrocytes to injury sites (Robel et al., 2011). We found a significant increase of Cdc42 and Rac1 activities in the protein extract from *Celsr2*$^{-/-}$ astrocytes upon stimulation by LPS-stimulated macrophage conditioned medium, and from *Celsr2*$^{-/-}$ spinal samples after SCI. In addition, inhibitors of Cdc42 or Rac1 efficiently reversed astrocyte morphological phenotypes induced by *Celsr2* inactivation in cultured cells. In addition, the administration of the inhibitors downregulated the activity of Cdc42 and Rac1, compromised astrocyte polarization and the improvement of lesion healing, axon regeneration and functional recovery in *Celsr2*$^{-/-}$ mice after SCI. Thus, Cdc42 and Rac1 are potential downstream molecules involved in the Celsr2-dependent motility of reactive astrocytes and neural repair, which is quite similar to the role in Celsr2-regulated axon regeneration of spinal motoneurons (Wen et al., 2022).

Polarized astrocytes may accelerate the compaction of lesion core and potentially promote healing after SCI. Reactive astrocyte polarization is inhibited by blocking β1-integrin or Wnt/β-catenin pathways and enhanced by the application of Wnt3a-Afamin complex after SCI (Sonn et al., 2020). Activation of canonical Wnt pathway using a GSK3 inhibitor after SCI efficiently limited lesion cavity, reduced demyelination, and enhanced functional recovery in mice (Renault-Mihara et al., 2011). STAT3 is another potential modulator of astrocyte polarity, as its conditional inactivation in astrocytes impaired protrusion elongation and lesion healing, accompanied with an increased spread of inflammatory cells and neuronal loss after SCI (Wanner et al., 2013). Our results further indicate that promoting astrocyte polarization by inactivating *Celsr2* might benefit neural repair after SCI. This is supported by the following findings: compared to control mice, *Celsr2*$^{-/-}$ animals had smaller lesion cavity, decreased glial scar area and higher fiber preservation in injured spinal cords, and showed improved recovery of motor and sensory function. We also found that regenerated serotoninergic fibers across lesion sites were more abundant in *Celsr2*$^{-/-}$ mice than in control animals.

In *Celsr2* cKO mice, in which tamoxifen induces inactivation of *Celsr2* in astrocytes immediately before and after SCI, behaviors of reactive astrocytes and the improvement of lesion healing, axonal regeneration and function recovery were similar to those in *Celsr2*$^{-/-}$ mice. This indicates that Celsr2 negatively modulates the mobility of reactive astrocytes in a cell-autonomous manner, and that inhibiting Celsr2 function in reactive astrocytes contributes to neural repair after SCI. Together with our recent report that Celsr2 inactivation is beneficial for axon regeneration, also in a cell autonomous manner (Wen et al., 2022), we propose that inhibiting Celsr2 will foster neural repair by enhancing intrinsic axon regeneration and ameliorating microenvironment simultaneously.

In addition, *Celsr2* inactivation contributes to the switch of functional phenotype of reactive astrocytes. Microglia-secreted cytokines (IL-1α, TNF-α and C1q) are strong inducers for A1 reactive astrocytes (Liddelow et al., 2017). When cultured spinal astrocytes were activated by the LPS-induced macrophage conditioned medium, the A1/A2 phenotype switch is confirmed by the downregulation of A1 astrocyte-related genes (*C3* and *Serping1*) and the upregulation of A2 astrocyte-related genes (*Clcf1*, *B3gnt5*, *Tm4sf1* and *Ptx3*) in *Celsr2*$^{-/-}$ samples. Immunostaining of injured spinal sections also indicates that *Celsr2* inactivation limits A1 phenotype of reactive astrocytes with lower C3 expression. Although *Celsr2* is not expressed in naïve microglial cells, the decrease of microglial response and alleviated neuroinflammation are identified in *Celsr2*$^{-/-}$ injured spinal cords, presumably via modulating astrocyte-microglia interactions. In the acute phase of SCI, reactive microglia proliferation was decreased and their ability to clear lipid drops was significantly increased in *Celsr2*$^{-/-}$ animals. We also found an upregulation of proinflammatory cytokine IL-3, which is produced by a subset of astrocytes and mediates astrocyte-microglia crosstalk (McAlpine et al., 2021), in *Celsr2*$^{-/-}$ injured spinal cords. In addition, downregulation of proinflammatory cytokines CCL4 and CCL5 were observed in injured spinal samples of *Celsr2*$^{-/-}$ animals. Decreased secretion of CCL4 and CCL5 could limit inflammatory cascade and local recruitment of inflammatory cells (Adamus et al., 2001; Luo et al., 2002). Altogether, our findings suggest that *Celsr2* inactivation promotes the astrocyte phenotype switch to alleviate neuroinflammation after SCI.

In conclusion, Celsr2 is an important modulator of morphological polarization and functional phenotypes of reactive astrocytes and inactivating *Celsr2* in astrocytes may be a potential therapeutic strategy for SCI.

AUTHOR CONTRIBUTIONS

Libing Zhou, Yibo Qu, Fadel Tissir, and Kwok-Fai So: designed the research project. Aimei Liu, Lingtai Yu, and Wei Zhang: performed animal studies and data analysis. Xuejun Li and Kejiang Zhang: performed

in vitro studies and data analysis. Aimei Liu and Libing Zhou: drafted the first version of the manuscript with input from Lingtai Yu, Xuejun Li, and Wei Zhang. Fadel Tissir, Yibo Qu, and Libing Zhou: reviewed and edited the manuscript. All authors read and approved the final manuscript.

ACKNOWLEDGMENTS

We wish to thank Prof. Tianming Gao for sharing mice. The work is supported by: National Natural Science Foundation of China (82271400 and 81971148, L. Zhou; 82222018, Y. Qu), Guangzhou Key Projects of Brain Science and Brain-Like Intelligence Technology (20200730009 and 20220600003, L. Zhou), Guangdong grant 'Key technologies for treatment of brain disorders' (2018B030332001, L. Zhou), Guangdong Basic and Applied Basic Research Foundation (2023B1515040015, Y. Qu), Programme of Introducing Talents of Discipline to Universities (B14036).

CONFLICT OF INTEREST STATEMENT

The authors declare no competing financial interests.

DATA AVAILABILITY STATEMENT

Primary data and materials described are available on reasonable request for academic use.

ORCID

Fadel Tissir https://orcid.org/0000-0002-9292-6622
Libing Zhou https://orcid.org/0000-0002-8975-5228

REFERENCES

Adamus, G., Manczak, M., & Machnicki, M. (2001). Expression of CC chemokines and their receptors in the eye in autoimmune anterior uveitis associated with EAE. *Investigative Ophthalmology & Visual Science*, *42*(12), 2894–2903.

Anderson, M. A., Burda, J. E., Ren, Y., Ao, Y., O'Shea, T. M., Kawaguchi, R., Coppola, G., Khakh, B. S., Deming, T. J., & Sofroniew, M. V. (2016). Astrocyte scar formation aids central nervous system axon regeneration. *Nature*, *532*(7598), 195–200. https://doi.org/10.1038/nature17623

Anderson, M. A., O'Shea, T. M., Burda, J. E., Ao, Y., Barlatey, S. L., Bernstein, A. M., Kim, J. H., James, N. D., Rogers, A., Kato, B., Wollenberg, A. L., Kawaguchi, R., Coppola, G., Wang, C., Deming, T. J., He, Z., Courtine, G., & Sofroniew, M. V. (2018). Required growth facilitators propel axon regeneration across complete spinal cord injury. *Nature*, *561*(7723), 396–400. https://doi.org/10.1038/s41586-018-0467-6

Assinck, P., Duncan, G. J., Hilton, B. J., Plemel, J. R., & Tetzlaff, W. (2017). Cell transplantation therapy for spinal cord injury. *Nature Neuroscience*, *20*(5), 637–647. https://doi.org/10.1038/nn.4541

Aung, W. Y., Mar, S., & Benzinger, T. L. (2013). Diffusion tensor MRI as a biomarker in axonal and myelin damage. *Imaging Med*, *5*(5), 427–440. https://doi.org/10.2217/iim.13.49

Bradbury, E. J., & Burnside, E. R. (2019). Moving beyond the glial scar for spinal cord repair. *Nature Communications*, *10*(1), 3879. https://doi.org/10.1038/s41467-019-11707-7

Britt, J. M., Kane, J. R., Spaeth, C. S., Zuzek, A., Robinson, G. L., Gbanaglo, M. Y., Estler, C. J., Boydston, E. A., Schallert, T., & Bittner, G. D. (2010). Polyethylene glycol rapidly restores axonal integrity and improves the rate of motor behavior recovery after sciatic nerve crush injury. *Journal of Neurophysiology*, *104*(2), 695–703. https://doi.org/10.1152/jn.01051.2009

Burda, J. E., & Sofroniew, M. V. (2014). Reactive gliosis and the multicellular response to CNS damage and disease. *Neuron*, *81*(2), 229–248. https://doi.org/10.1016/j.neuron.2013.12.034

Bush, T. G., Puvanachandra, N., Horner, C. H., Polito, A., Ostenfeld, T., Svendsen, C. N., Mucke, L., Johnson, M. H., & Sofroniew, M. V. (1999). Leukocyte infiltration, neuronal degeneration, and neurite outgrowth after ablation of scar-forming, reactive astrocytes in adult transgenic mice. *Neuron*, *23*(2), 297–308. https://doi.org/10.1016/s0896-6273(00)80781-3

Camand, E., Peglion, F., Osmani, N., Sanson, M., & Etienne-Manneville, S. (2012). N-cadherin expression level modulates integrin-mediated polarity and strongly impacts on the speed and directionality of glial cell migration. *Journal of Cell Science*, *125*(Pt 4), 844–857. https://doi.org/10.1242/jcs.087668

Chaker, D., Mouawad, C., Azar, A., Quilliot, D., Achkar, I., Fajloun, Z., & Makdissy, N. (2018). Inhibition of the RhoGTPase Cdc42 by ML141 enhances hepatocyte differentiation from human adipose-derived mesenchymal stem cells via the Wnt5a/PI3K/miR-122 pathway: Impact of the age of the donor. *Stem Cell Research & Therapy*, *9*(1), 167. https://doi.org/10.1186/s13287-018-0910-5

Escartin, C., Galea, E., Lakatos, A., O'Callaghan, J. P., Petzold, G. C., Serrano-Pozo, A., Steinhauser, C., Volterra, A., Carmignoto, G., Agarwal, A., Allen, N. J., Araque, A., Barbeito, L., Barzilai, A., Bergles, D. E., Bonvento, G., Butt, A. M., Chen, W. T., Cohen-Salmon, M., … Verkhratsky, A. (2021). Reactive astrocyte nomenclature, definitions, and future directions. *Nature Neuroscience*, *24*(3), 312–325. https://doi.org/10.1038/s41593-020-00783-4

Etienne-Manneville, S., & Hall, A. (2001). Integrin-mediated activation of Cdc42 controls cell polarity in migrating astrocytes through PKCzeta. *Cell*, *106*(4), 489–498. https://doi.org/10.1016/s0092-8674(01)00471-8

Feng, J., Han, Q., & Zhou, L. (2012). Planar cell polarity genes, Celsr1-3, in neural development. *Neuroscience Bulletin*, *28*(3), 309–315. https://doi.org/10.1007/s12264-012-1232-8

Freeman, M. R. (2010). Specification and morphogenesis of astrocytes. *Science*, *330*(6005), 774–778. https://doi.org/10.1126/science.1190928

Fukata, M., Nakagawa, M., & Kaibuchi, K. (2003). Roles of Rho-family GTPases in cell polarisation and directional migration. *Current Opinion in Cell Biology*, *15*(5), 590–597. https://doi.org/10.1016/s0955-0674(03)00097-8

Ghosh, M., & Pearse, D. D. (2014). The role of the serotonergic system in locomotor recovery after spinal cord injury. *Front Neural Circuits*, *8*. https://doi.org/10.3389/fncir.2014.00151

Goffinet, A. M., & Tissir, F. (2017). Seven pass Cadherins CELSR1-3. *Seminars in Cell & Developmental Biology*, *69*, 102–110. https://doi.org/10.1016/j.semcdb.2017.07.014

Gray, R. S., Roszko, I., & Solnica-Krezel, L. (2011). Planar cell polarity: Coordinating morphogenetic cell behaviors with embryonic polarity. *Developmental Cell*, *21*(1), 120–133. https://doi.org/10.1016/j.devcel.2011.06.011

Hu, N. Y., Chen, Y. T., Wang, Q., Jie, W., Liu, Y. S., You, Q. L., Li, Z. L., Li, X. W., Reibel, S., Pfrieger, F. W., Yang, J. M., & Gao, T. M. (2020). Expression patterns of inducible Cre recombinase driven by differential astrocyte-specific promoters in transgenic mouse lines. *Neuroscience Bulletin*, *36*(5), 530–544. https://doi.org/10.1007/s12264-019-00451-z

Jiang, C., Sun, Z. M., Zhu, D. C., Guo, Q., Xu, J. J., Lin, J. H., Chen, Z. X., & Wu, Y. S. (2020). Inhibition of Rac1 activity by NSC23766 prevents cartilage endplate degeneration via Wnt/beta-catenin pathway. *Journal of Cellular and Molecular Medicine*, *24*(6), 3582–3592. https://doi.org/10.1111/jcmm.15049

Jo, M., Kim, J. H., Song, G. J., Seo, M., Hwang, E. M., & Suk, K. (2017). Astrocytic Orosomucoid-2 modulates microglial activation and Neuroinflammation. *The Journal of Neuroscience*, *37*(11), 2878–2894. https://doi.org/10.1523/JNEUROSCI.2534-16.2017

Karimi-Abdolrezaee, S., & Billakanti, R. (2012). Reactive astrogliosis after spinal cord injury-beneficial and detrimental effects. *Molecular Neurobiology*, *46*(2), 251–264. https://doi.org/10.1007/s12035-012-8287-4

Koopmans, G. C., Deumens, R., Honig, W. M., Hamers, F. P., Steinbusch, H. W., & Joosten, E. A. (2005). The assessment of locomotor function in spinal cord injured rats: The importance of objective analysis of coordination. *Journal of Neurotrauma*, *22*(2), 214–225. https://doi.org/10.1089/neu.2005.22.214

Lagos-Cabre, R., Brenet, M., Diaz, J., Perez, R. D., Perez, L. A., Herrera-Molina, R., Quest, A. F. G., & Leyton, L. (2018). Intracellular Ca(2+) increases and Connexin 43 Hemichannel opening are necessary but not sufficient for Thy-1-induced astrocyte migration. *International Journal of Molecular Sciences*, *19*(8), 2179. https://doi.org/10.3390/ijms19082179

Lehmann, H. C., Zhang, J., Mori, S., & Sheikh, K. A. (2010). Diffusion tensor imaging to assess axonal regeneration in peripheral nerves. *Experimental Neurology*, *223*(1), 238–244. https://doi.org/10.1016/j.expneurol.2009.10.012

Li, Z., Wu, J., Zhang, X., Ou, C., Zhong, X., Chen, Y., Lu, L., Liu, H., Li, Y., Liu, X., Wu, B., Wang, Y., Yang, P., Yan, J., & Chen, M. (2019). CDC42 promotes vascular calcification in chronic kidney disease. *The Journal of Pathology*, *249*(4), 461–471. https://doi.org/10.1002/path.5334

Liao, J., Ye, Z., Huang, G., Xu, C., Guo, Q., & Wang, E. (2014). Delayed treatment with NSC23766 in streptozotocin-induced diabetic rats ameliorates post-ischemic neuronal apoptosis through suppression of mitochondrial p53 translocation. *Neuropharmacology*, *85*, 508–516. https://doi.org/10.1016/j.neuropharm.2014.06.008

Liddelow, S. A., Guttenplan, K. A., Clarke, L. E., Bennett, F. C., Bohlen, C. J., Schirmer, L., Bennett, M. L., Munch, A. E., Chung, W. S., Peterson, T. C., Wilton, D. K., Frouin, A., Napier, B. A., Panicker, N., Kumar, M., Buckwalter, M. S., Rowitch, D. H., Dawson, V. L., Dawson, T. M., … Barres, B. A. (2017). Neurotoxic reactive astrocytes are induced by activated microglia. *Nature*, *541*(7638), 481–487. https://doi.org/10.1038/nature21029

Luo, Y., Berman, M. A., Zhai, Q., Fischer, F. R., Abromson-Leeman, S. R., Zhang, Y., Kuziel, W. A., Gerard, C., & Dorf, M. E. (2002). RANTES stimulates inflammatory cascades and receptor modulation in murine astrocytes. *Glia*, *39*(1), 19–30. https://doi.org/10.1002/glia.10079

McAlpine, C. S., Park, J., Griciuc, A., Kim, E., Choi, S. H., Iwamoto, Y., Kiss, M. G., Christie, K. A., Vinegoni, C., Poller, W. C., Mindur, J. E., Chan, C. T., He, S., Janssen, H., Wong, L. P., Downey, J., Singh, S., Anzai, A., Kahles, F., … Swirski, F. K. (2021). Astrocytic interleukin-3 programs microglia and limits Alzheimer's disease. *Nature*, *595*(7869), 701–706. https://doi.org/10.1038/s41586-021-03734-6

Okada, S., Nakamura, M., Katoh, H., Miyao, T., Shimazaki, T., Ishii, K., Yamane, J., Yoshimura, A., Iwamoto, Y., Toyama, Y., & Okano, H. (2006). Conditional ablation of Stat3 or Socs3 discloses a dual role for reactive astrocytes after spinal cord injury. *Nature Medicine*, *12*(7), 829–834. https://doi.org/10.1038/nm1425

O'Shea, T. M., Burda, J. E., & Sofroniew, M. V. (2017). Cell biology of spinal cord injury and repair. *The Journal of Clinical Investigation*, *127*(9), 3259–3270. https://doi.org/10.1172/JCI90608

Osmani, N., Vitale, N., Borg, J. P., & Etienne-Manneville, S. (2006). Scrib controls Cdc42 localization and activity to promote cell polarization during astrocyte migration. *Current Biology*, *16*(24), 2395–2405. https://doi.org/10.1016/j.cub.2006.10.026

Petrova, V., & Hakim, S. (2022). CELSR2, a new player in motor neuron axon growth and regeneration. *Brain*, *145*, 420–422. https://doi.org/10.1093/brain/awac021

Qu, Y., Glasco, D. M., Zhou, L., Sawant, A., Ravni, A., Fritzsch, B., Damrau, C., Murdoch, J. N., Evans, S., Pfaff, S. L., Formstone, C., Goffinet, A. M., Chandrasekhar, A., & Tissir, F. (2010). Atypical cadherins Celsr1-3 differentially regulate migration of facial branchiomotor neurons in mice. *The Journal of Neuroscience*, *30*(28), 9392–9401.

Qu, Y., Huang, Y., Feng, J., Alvarez-Bolado, G., Grove, E. A., Yang, Y., Tissir, F., Zhou, L., & Goffinet, A. M. (2014). Genetic evidence that Celsr3 and Celsr2, together with Fzd3, regulate forebrain wiring in a Vangl-independent manner. *Proceedings of the National Academy of Sciences of the United States of America*, *111*(29), E2996–E3004. https://doi.org/10.1073/pnas.1402105111

Renault-Mihara, F., Katoh, H., Ikegami, T., Iwanami, A., Mukaino, M., Yasuda, A., Nori, S., Mabuchi, Y., Tada, H., Shibata, S., Saito, K., Matsushita, M., Kaibuchi, K., Okada, S., Toyama, Y., Nakamura, M., & Okano, H. (2011). Beneficial compaction of spinal cord lesion by migrating astrocytes through glycogen synthase kinase-3 inhibition. *EMBO Molecular Medicine*, *3*(11), 682–696. https://doi.org/10.1002/emmm.201100179

Robel, S., Bardehle, S., Lepier, A., Brakebusch, C., & Gotz, M. (2011). Genetic deletion of cdc42 reveals a crucial role for astrocyte recruitment to the injury site in vitro and in vivo. *The Journal of Neuroscience*, *31*(35), 12471–12482. https://doi.org/10.1523/JNEUROSCI.2696-11.2011

Santello, M., Toni, N., & Volterra, A. (2019). Astrocyte function from information processing to cognition and cognitive impairment. *Nature Neuroscience*, *22*(2), 154–166. https://doi.org/10.1038/s41593-018-0325-8

Silver, J., & Miller, J. H. (2004). Regeneration beyond the glial scar. *Nature Reviews. Neuroscience*, *5*(2), 146–156. https://doi.org/10.1038/nrn1326

Sonn, I., Nakamura, M., Renault-Mihara, F., & Okano, H. (2020). Polarization of reactive astrocytes in response to spinal cord injury is enhanced by M2 macrophage-mediated activation of Wnt/beta-catenin pathway. *Molecular Neurobiology*, *57*(4), 1847–1862. https://doi.org/10.1007/s12035-019-01851-y

Souza, D. G., Almeida, R. F., Souza, D. O., & Zimmer, E. R. (2019). The astrocyte biochemistry. *Seminars in Cell & Developmental Biology*, *95*, 142–150. https://doi.org/10.1016/j.semcdb.2019.04.002

Su, Y., Chen, Z., Du, H., Liu, R., Wang, W., Li, H., & Ning, B. (2019). Silencing miR-21 induces polarization of astrocytes to the A2 phenotype and improves the formation of synapses by targeting glypican 6 via the signal transducer and activator of transcription-3 pathway after acute ischemic spinal cord injury. *The FASEB Journal*, *33*(10), 10859–10871. https://doi.org/10.1096/fj.201900743R

Tissir, F., Qu, Y., Montcouquiol, M., Zhou, L., Komatsu, K., Shi, D., Fujimori, T., Labeau, J., Tyteca, D., Courtoy, P., Poumay, Y., Uemura, T., & Goffinet, A. M. (2010). Lack of cadherins Celsr2 and Celsr3 impairs ependymal ciliogenesis, leading to fatal hydrocephalus. *Nature Neuroscience*, *13*(6), 700–707. https://doi.org/10.1038/nn.2555

Vismara, I., Papa, S., Veneruso, V., Mauri, E., Mariani, A., De Paola, M., Affatato, R., Rossetti, A., Sponchioni, M., Moscatelli, D., Sacchetti, A., Rossi, F., Forloni, G., & Veglianese, P. (2020). Selective modulation of A1 astrocytes by drug-loaded Nano-structured gel in spinal cord injury. *ACS Nano*, *14*(1), 360–371. https://doi.org/10.1021/acsnano.9b05579

Wanner, I. B., Anderson, M. A., Song, B., Levine, J., Fernandez, A., Gray-Thompson, Z., Ao, Y., & Sofroniew, M. V. (2013). Glial scar borders are formed by newly proliferated, elongated astrocytes that interact to corral inflammatory and fibrotic cells via STAT3-dependent mechanisms after spinal cord injury. *The Journal of Neuroscience*, *33*(31), 12870–12886. https://doi.org/10.1523/JNEUROSCI.2121-13.2013

Wen, Q., Weng, H., Liu, T., Yu, L., Zhao, T., Qin, J., Li, S., Wu, Q., Tissir, F., Qu, Y., & Zhou, L. (2022). Inactivating Celsr2 promotes motor axon fasciculation and regeneration in mouse and human. *Brain*, *145*(2), 670–683. https://doi.org/10.1093/brain/awab317

Yang, T., Dai, Y., Chen, G., & Cui, S. (2020). Dissecting the dual role of the glial scar and scar-forming astrocytes in spinal cord injury. *Frontiers in Cellular Neuroscience*, *14*. https://doi.org/10.3389/fncel.2020.00078

Zhang, Y., Sloan, S. A., Clarke, L. E., Caneda, C., Plaza, C. A., Blumenthal, P. D., … Barres, B. A. (2016). Purification and characterization of progenitor and mature human astrocytes reveals transcriptional and functional differences with mouse. *Neuron*, *89*(1), 37–53. https://doi.org/10.1016/j.neuron.2015.11.013

Zhou, L., Bar, I., Achouri, Y., Campbell, K., De Backer, O., Hebert, J. M., Jones, K., Kessaris, N., de Rouvroit, C. L., O'Leary, D., Richardson, W. D., Goffinet, A. M., & Tissir, F. (2008). Early forebrain wiring: Genetic dissection using conditional Celsr3 mutant mice. *Science*, *320*(5878), 946–949. https://doi.org/10.1126/science.1155244

SUPPORTING INFORMATION

Additional supporting information can be found online in the Supporting Information section at the end of this article.

How to cite this article: Liu, A., Yu, L., Li, X., Zhang, K., Zhang, W., So, K.-F., Tissir, F., Qu, Y., & Zhou, L. (2023). Celsr2-mediated morphological polarization and functional phenotype of reactive astrocytes in neural repair. *Glia*, *71*(8), 1985–2004. https://doi.org/10.1002/glia.24378